Soil Dynamics and Earthquake Engineering 178 (2024) 108450

Contents lists available at ScienceDirect

Soil Dynamics and Earthquake Engineering

journal homepage: www.elsevier.com/locate/soildyn

Multi-disciplinary performance comparison for selecting the optimal sustainable design of buildings structures with fluid-viscous dampers

Ali Rodríguez-Castellanos [a], Mauro Niño [a,*], Sonia E. Ruiz [b], Marco A. Santos Santiago [b]

[a] UNAM, Facultad de Ingeniería, Av. Universidad No. 3000, Del. Coyoacán, Ciudad de México, CP, 04510, Mexico
[b] UNAM, Instituto de Ingeniería, Av. Universidad No. 3000, Del. Coyoacán, Ciudad de México, CP, 04510, Mexico

ARTICLE INFO

Keywords:
Sustainable seismic design
FEMA P-58
Viscous damping
Environmental impact

ABSTRACT

Earthquake engineering aims to control the building performance and viscous damping systems are recognized for enhancing the seismic performance; however, performance is often assessed economically over other critical metrics. This study evaluates the seismic building performance with fluid viscous dampers from a sustainability perspective: economy, social factors, and environmental impact. It also identifies the optimal sustainable design considering the damping parameters α and C of the energy dissipation devices. Thus, a set of 28-story buildings equipped with viscous dampers is designed, where the damping properties (*i.e.*, α and C) are varied to produce different structural alternatives. The FEMA P-58 methodology is utilized for evaluating the performance of the case studies. Then, the optimal design is defined as the building associated with the damping properties that minimize the expected annual loss considering repair costs, injuries, and carbon emissions. Results demonstrate that proper damping parameters selection significantly reduces expected annual losses compared to structures without supplemental damping system.

1. Introduction

Seismic codes for earthquake-resistant design of structures generate structural designs that can withstand a broad range of static and dynamic loads. Moreover, their goal is to avoid the collapse of structures subjected to high-intensity seismic event. Evidently, the objective is to promote life safety over the preservation of the structure [1,2]. Nevertheless, complying with the codes requirements does not necessarily guarantee the prevention of significant financial losses due to the structural damage induced by a specific seismic event. Currently, earthquake engineering employs performance-based methodologies for the earthquake-resistant design of buildings. These methodologies involve estimating and, even, controlling the performance of structures through discrete performance levels (*e.g.*, operational, immediate occupancy, life safety, and collapse prevention) [3–6]. The previous approach allows quantification and delimitation of damage that a building may sustain when subjected to a particular seismic intensity level. However, stakeholders (*e.g.*, owners, investors, developers, insurance companies, etc.) are not explicitly informed about the economic consequences of repair activities or the resulting downtime, much less the number of injuries or deaths that could occur due to seismic design actions or extraordinary seismic events.

Furthermore, it is widely recognized that the construction industry substantially contributes to the depletion of natural resources and affects the environment through the emission of greenhouse gases and waste generation [7–10]. It is estimated that the construction sector is responsible for approximately 40 % of global greenhouse gas emissions (embodied carbon) annually [11]. Moreover, when a natural disaster such as a seismic event occurs, repairing activities generate additional carbon emissions due to the extraction of materials and their implementation to restore the building to its original shape. Therefore, building projects are nowadays under public scrutiny regarding their environmental impact. As a result, earthquake engineering has begun to prioritize the integration of environmental impact associated with repair and/or rehabilitation actions as a performance measure. The previous empowers stakeholders to make design decisions from an environmental-conscious perspective. Studies indicate that the consumption of embodied energy (which encompasses the extraction of raw materials, manufacturing of construction materials, transportation, waste generation, etc.) used for repair actions resulting from structural damage caused by a specific seismic event may represent up to 30 % of the environmental impact generated during the initial construction

* Corresponding author.
E-mail address: mninol@ingenieria.unam.edu (M. Niño).

https://doi.org/10.1016/j.soildyn.2024.108450
Received 17 May 2023; Received in revised form 30 November 2023; Accepted 1 January 2024
Available online 6 January 2024

phase [7,12–14].

Advanced methodologies in performance-based seismic design expand the current approach, providing understandable metrics for stakeholders to influence the final building design. The Federal Emergency Management Agency (FEMA) recently introduced a methodology for assessing the seismic performance of buildings contained in FEMA P-58 [15]. This methodology probabilistically expresses the seismic performance of a building in terms of repair costs, repair time, number of casualties (injuries and/or deaths), environmental impact, and unsafe placarding, known as performance measures. Simultaneously, this methodology promotes *sustainable seismic design*, aiming for a balance in building performance across economic, social, and environmental aspects [16–19]. Recent research has applied this methodology to evaluate various structural systems, primarily focusing on economic losses. Systems include reinforced concrete frame structures [20], steel concentrically braced frame structures [21], steel buckling restrained braced frame structures [22], steel moment-resisting frame structures [23], and masonry buildings [24], with a few exceptions embracing the complete methodology [25].

On the other hand, building structures equipped with fluid viscous damping system are recognized for enhancing their seismic performance [26–29]. Implementing these systems involves specifying the properties of the viscous dampers, α and C, related to its non-linear nature and damping constant, respectively. These devices are an appealing alternative to control the seismic damage in a building, providing supplementary damping, limiting interstory drift, and acting as fuse elements by dissipating seismic energy through viscous liquids. Similarly, like other structural systems mentioned above, their performance evaluation using FEMA P-58 methodology [15] primarily focuses on monetary losses and remains limited [30–33]. Consequently, it has not been assessed casualties or carbon emissions resulting from repair actions in buildings equipped with viscous dampers subjected to earthquake events.

The objective of the present study is to assess the seismic performance of buildings with fluid viscous dampers and identify the most sustainable design based on the properties of these energy dissipation devices (α and C). This assessment is conducted for a set of 28-story buildings equipped with fluid viscous dampers located in Acapulco, Guerrero, Mexico, where the properties of the energy dissipation devices (*i.e.*, α and C) are varied to produce different structural designs with unique dynamic responses. FEMA P-58 methodology [15] is used for the performance evaluation of each design, considering the three dimensions of sustainability: repair costs (economy), number of serious injuries (social), and carbon emissions (environmental impact). Subsequently, the optimal design is selected based on sustainability criteria, focusing on the building structure design associated with damping exponent α that yields the lowest expected annual loss in terms of repair costs, number of serious injuries, and carbon emissions.

2. Methodology

Phase 1. To achieve the stated objective, the first step focuses on designing a set of 28-story buildings outfitted with viscous fluid dampers, including the location and definition of the α and C values of the viscous dampers. Several pioneering works have contributed to the research on the optimal design, placement, and sizing of viscous dampers over the past decades [34–39]. Detailed methodologies for the optimal design and placement of viscous dampers in building structures are comprehensively described in Refs. [40–43]. However, while these methods may lead to an optimal damper configuration, their complexity can sometimes make them impractical to be routinely used by engineers. Consequently, practical methodologies for seismic design with viscous damper devices in building structures have been proposed [44–51]. Moreover, various countries have published seismic design guidelines offering simplified methods based on spectral modal analysis and equivalent lateral forces for buildings with passive energy dissipation devices [1,2,52–54].

In present research, the design of the case of studies follows the recommendations established in chapter 18 of the American Society of Civil Engineers standards (ASCE/SEI 7–16) [1], including some adaptations set forth in the Manual for Civil Structures Design by the Federal Commission of Electricity of Mexico (MCSD-CFE, acronym in Spanish) [55], and the consideration of the influence of higher modes of vibration according to Santos et al., [56]. This approach is based on spectral modal analysis and enables the determination, through an iterative process, of the parameters of the constitutive law that define the hysteretic behavior of the fluid viscous damping devices (Eq. (1)) [57]:

$$F_D = C|V|^{\alpha} sgn(V) \tag{1}$$

where F_D represents the force of the damper. The damping exponent α is related to the nonlinearity of the viscous damper, while C is the damping constant. The term V represents the relative velocity acting on the damper, and $sgn(V)$ is the sign function applied to the relative velocity.

The designer is responsible for determining the characteristics of the viscous damping devices, that is, the values of constant C and the exponent α, based on the dynamic properties of the structure. In this study, these properties (*i.e.*, α and C) are varied to establish different design alternatives. Typically, C is iteratively computed for a given value of α until the desired damping level is attained [58–61]. Basically, the design process begins with a predesign of the structural system using the spectral modal method. In this method, the design spectrum is adjusted by a damping factor (β) to account for the presence of viscous dampers [55]. This factor is determined by the ratio of critical effective damping (ζ), which encompasses both inherent structural and viscous damping, and the fundamental vibration period of the building (T_1) [55]. The results of the spectral analysis (*i.e.*, vibration period, mode shapes, interstory drifts, interstory velocities) are used to determine the damping constant C based on an energetic approach [1]. This approach focusses on establishing the relationship between the energy dissipated over a full cycle of the viscous damper set and the strain energy experienced by the structural system at its maximum displacement [1].

In this study, the damping constant C remains the same for all stories associated with a given damping exponent α. Additionally, simplified design methods are not permitted by some seismic design codes for high-rise buildings. To verify the correct structural behavior of the designs, dynamic nonlinear analyses using ten synthetic accelerograms that match the design spectrum were conducted according to ASCE/SEI 7–16 and MCSD-CFE [1,55].

As mentioned earlier, this study explores different values of α and then calculates the corresponding damping constant C. However, although simplified methods assist to define the parameters of the constitutive law of viscous damping devices, the challenge lies in finding the optimal values of C and α for the viscous damping devices, since even if the strength and deformation demands of the structure are satisfied, there is no guarantee that the characteristics selected for such devices are optimal from a financial, social, and environmental perspective.

Phase 2. In light of the above, this stage involves evaluating the performance of the structure in terms of economic losses, environmental impact (carbon emissions), and the number of injuries. Subsequently, to determine the optimal α and C values that minimize the expected annual losses. To accomplish this, the FEMA P-58 methodology is used [15], which is based on the formulation developed by the Pacific Earthquake Engineering Research Center (PEER) [62–64]. The PEER formulation, through the total probability theorem, calculates the consequences originated by the seismic action in terms of the probability of incurring in specific values of performance measures (*e.g.*, repair costs, number of casualties, environmental impact, etc.). In this regard, this approximation can be expressed as the triple integral shown below [63]:

$$\lambda(DV) = \int_{im}\int_{dm}\int_{edp} G(DV|DM)dG(DM|EDP)dG(EDP|IM)|d\lambda(IM)| \tag{2}$$

where $G(x|y)$ is the complementary cumulative distribution function of a random variable X given that the random variable Y takes a value equal to y. Therefore, $dG(x|y)$ represents the derivative of such distribution function. On the other hand, $\lambda(x)$ is the mean ratio at which a random variable X exceeds a certain value x per unit of time. DV is the decision or consequence variable (*e.g.*, repair costs, casualties, etc.); DM is the damage measure associated with the building response; EDP is the demand parameter that characterizes both the structural and the non-structural response (*e.g.*, story distortions, floor acceleration, etc.); IM is the intensity measure used to describe the hazard of a seismic event (*e.g.*, $Sa(T_1)$, PGA, etc.). When equation (2) is examined, it becomes apparent that the PEER formulation consists of the following analyses: *damage analysis*, *loss analysis*, *seismic hazard analysis*, and *structural response analysis*. On the other hand, the FEMA P-58 methodology consists of the following steps:

Step 1. Building performance model. Constructing a performance model involves gathering data that can be used to determine the vulnerability of the components of a building (*e.g.*, structural, and non-structural elements), and the corresponding consequences, such as economic losses, environmental impact, and the number of casualties. This stage requires information that can be used to specify the distribution of damage in the components that make up a building given a demand level, $G(DM|EDP)$ (*i.e.*, fragility functions) and to establish the distribution of the consequence variable given the level of damage reached $G(DV|DM)$ (*i.e.*, consequence functions). Thus, the construction of the performance model addresses both the *damage analysis* and *loss analysis* of equation (2). This stage also includes collecting initial data related to the building dimensions, replacement costs, construction time, environmental impact, and occupancy conditions as well as developing a model that characterizes the distribution of the number of people inside the building.

Step 2. Seismic hazard definition. To determine the seismic hazard of a particular site, the FEMA P-58 methodology [15] suggests a probabilistic seismic hazard analysis. Conceptually, this analysis combines the probabilities corresponding that a specific intensity measure, IM, exceeds a certain level of intensity, im, given the occurrence of seismic events with potential magnitudes and locations associated with each seismic zone that influences the seismic hazard of the site. This combination results in seismic hazard curves that represent the annual probability of exceeding a specific intensity level for a given structural period. At this stage, suitable seismic records are also selected for use in subsequent nonlinear time-history analyses. It is crucial that these selected ground motion records are consistent with the seismic hazard analysis performed, which means using seismic records that can potentially generate the desired intensity value identified in the hazard curve. This phase specifically addresses the *seismic hazard analysis*, $\lambda(IM)$, outlined in equation (2).

Step 3. Analysis of the building response. The building response analysis stage involves evaluating how a structure responds to a particular seismic action and identifying the structural demand parameters associated with damage to building components. The demand parameters commonly used to characterize damage are interstory drift and floor acceleration. FEMA P-58 [15] presents two methods to estimate these parameters: a) the simplified method based on the ASCE 41-17 provisions for linear static analysis [6], and b) the nonlinear time-history analysis, with the latter being used in this study. This stage addresses the *structural response analysis*, $G(EDP|IM)$, specified in equation (2). The goal is to assemble a matrix that represents the structural demand values obtained from an analysis associated with a particular intensity and demand parameters estimated at specific locations in the building (*e.g.*, interstory drift at the second level with a N–S direction). This matrix is used to generate a set of simulated demands, which are then used to determine the building performance.

Step 4. Definition of fragility to collapse. The collapse of a building is the primary cause of fatalities or injuries during a seismic event. Therefore, it is essential to determine the probability of structural collapse to evaluate performance from this perspective. To achieve this, the collapse fragility curve can be estimated, which indicates the probability of building collapse at a particular level of intensity. Various methods for obtaining the collapse fragility curve are presented in FEMA P-58 [15], with incremental dynamic analysis (IDA) being the most accurate approach [65]. IDAs involve conducting a series of nonlinear analyses at multiple intensity levels to produce responses ranging from linear to those that result in the collapse of the structure. This stage also involves defining collapse modes and their probability of occurrence, as well as determining the affected area and the corresponding likelihood of injury or fatalities in those areas.

Step 5. Performance calculation. The FEMA P-58 methodology [15] uses the Monte Carlo method and a matrix of simulated demands (called realizations) to evaluate the seismic performance of structures and consider the inherent uncertainties in their estimation. The performance calculation begins with the first realization and determines whether the structure collapses or not. In case of collapse, the losses are associated with replacement values. Otherwise, the level of damage is evaluated, and the corresponding losses are computed. This process is repeated for multiple realizations, and the losses are sorted to obtain a distribution function of the decision variable of interest. To facilitate the process, a software called Performance Assessment Calculation Tool (PACT) is used. PACT [66] is an electronic tool and repository of fragility and consequence functions that performs the probabilistic and loss accumulation calculations described in the FEMA P-58 methodology [15]. In this research, PACT was used for all probabilistic calculations.

3. Environmental impact

Although the *Building performance model* step implicitly includes quantifying the environmental impact, this process is explained in detail here. Environmental impact refers to changes in the environment caused by human activity or natural events. The FEMA P-58 methodology [15] utilizes two metrics to characterize the environmental impact: equivalent carbon dioxide emissions (kg-CO2eq) and the energy required for material production (MJ), also known as embodied carbon and embodied energy. A life cycle analysis (LCA) is used to determine the potential environmental impact of a product or process during a specific stage or its entire lifespan.

The FEMA P-58 methodology [15] quantifies the environmental impact resulting from the repair actions required to restore a building to its pre-seismic damage condition. This is achieved directly from the repair cost estimates in combination with the Economic Input-Output life cycle assessment (EIO-LCA). This model associates the amount of money spent by the industrial sectors that conform the economy of a country with the environmental impact generated by their operations. The procedure consists of the following steps: 1) estimate the resulting costs of the repair actions carried out to restore damage induced by a seismic event; 2) identify the industrial sectors involved in restoration activities and their corresponding environmental impact factors per dollar spent (*e.g.*, 0.50 kg CO2eq/US$); 3) break down the estimated repair costs and assign them to the different industrial sectors identified previously; 4) add the costs associated with each industrial sector; and 5) multiply the cost obtained in each industrial sector by its corresponding impact factor, and then add the impact of all sectors to obtain the total environmental impact. It is recognized that the EIO-LCA may overestimate the environmental impact, yielding conservative estimates. This aligns well with the precision level of the FEMA P-58 methodology in its current state of development. Further information regarding the discussed topic can be found elsewhere [67,68].

The FEMA P-58 methodology [15] also needs to establish replacement quantities based on the environmental impact associated with the initial construction stage of the building (in case of collapse), which is analogous to estimate the total replacement cost, as discussed in subsequent sections. Therefore, embodied carbon and embodied energy must be estimated a priory. In this study, replacement quantities were determined using a simplified EIO-LCA. This approach is simpler but less precise, enabling the analysis without requiring comprehensive data on the inventory of the structure and construction costs. Instead, the total cost of the building is multiplied by an environmental impact factor related to constructing a building for a particular occupancy purpose (*e.g.*, commercial office, healthcare, hospitality, etc.)

Several databases [69,70] contain environmental impact factors that link to the amount of money spent in various industrial sectors present in the economy of a country. They also provide impact factors for building construction based on occupancy type. The FEMA P-58 methodology [15] uses the database developed by Yang et al. [70] to estimate the environmental impacts after calculating repair costs given the damage state in the different building components (*i.e.*, structural and no structural elements). This database relates the economic interactions of different industrial sectors in the United States (US) with their environmental emissions and offers environmental impact factors associated with the construction of buildings with various occupancy purposes.

In developing countries like Mexico, there is a lack of adequate data to assess the environmental impact in the construction sector [71,72]. As a result, life cycle inventories from developed countries are often used to evaluate the environmental impact of buildings [71,73–75]. To overcome this limitation, this study employs the environmental impact values available in the PACT database [66], which is based on the model developed by Yang et al. [70]. Furthermore, the Yang et al. [70] model is used to estimate replacement quantities associated with carbon emissions and embodied energy during the initial construction phase of the structure. In addition, only carbon emissions (embodied carbon/greenhouse gases/potential for global warming) are considered for the environmental impact assessment. It is noteworthy that equivalent of CO_2 has been identified as a good predictor of other relevant environmental impact indicators when evaluating the impact of repair actions on earthquake-damaged buildings [76].

4. Phase 1: design of the case studies

Mexico experiences numerous seismic events annually, with the Pacific coast being the region that suffers the most. According to the National Seismological Service [77], 80 % of earthquakes recorded in 2021 and 2022 occurred in this area. As a result, the construction of structures in this region is controlled by lateral forces generated during seismic events. Therefore, this study assumes that the building under consideration is located in the port of Acapulco, Guerrero, and is intended to be used as a hotel.

The case studies were based on a 28-story building with a steel-concrete composite frame system. The dimensions of the building structure are shown in Fig. 1a and b, and the location of the viscous damping devices is depicted in Fig. 1c. To regulate the flexural behavior of the building, a diagonal brace system (outrigger) has been added on stories 15 and 28, both in the longitudinal and transverse directions. This system enhances the stability and strength of the building, reducing lateral drifts from earthquakes and wind loads [78]. No effort was made to assess the seismic performance, with or without an outrigger system; however, further insights into the benefits that the outrigger system offers for structural performance can be found in other sources [79]. The seismic design of the structure was initially carried out conventionally, following the earthquake design guidelines presented in the MCSD-CFE [55]. This preliminary design, without the consideration of a supplementary damping system, was referred to as the "conventional building".

Subsequently, the buildings with fluid viscous damping devices were designed using a simplified method based on spectral modal analysis, as recommended by previous research studies [1,2,58,61]. Several simplified analyses were conducted, varying the exponent α from 0.1 to 1.0 in increments of 0.1. The constant C (see Equation (1)) was then determined to achieve an effective damping of 20 % of the critical damping.

As a result, ten additional case studies were generated in addition to the conventional building. These case studies were identified with letter "E" followed by the value of exponent α. For example, E−01 corresponds to the building with α equal to 0.1, E−00 refers to the conventional structure without energy dissipation devices, and E−10 represents the building with a linear viscous damping system when α is equal to 1.0. The design of the building with and without energy dissipation devices was executed with ETABS 18 software [80].

Tables 1–5 present the resulting sections for the conventional building and those with supplementary damping devices. It is observed that beam dimensions vary with building height. This variation is a result of compliance with Mexican seismic design guidelines [2,55], which recommend that beams integrated into the seismic force-resisting system must contribute to the earthquake resistance and stiffness for controlling building displacements. Furthermore, a superscript

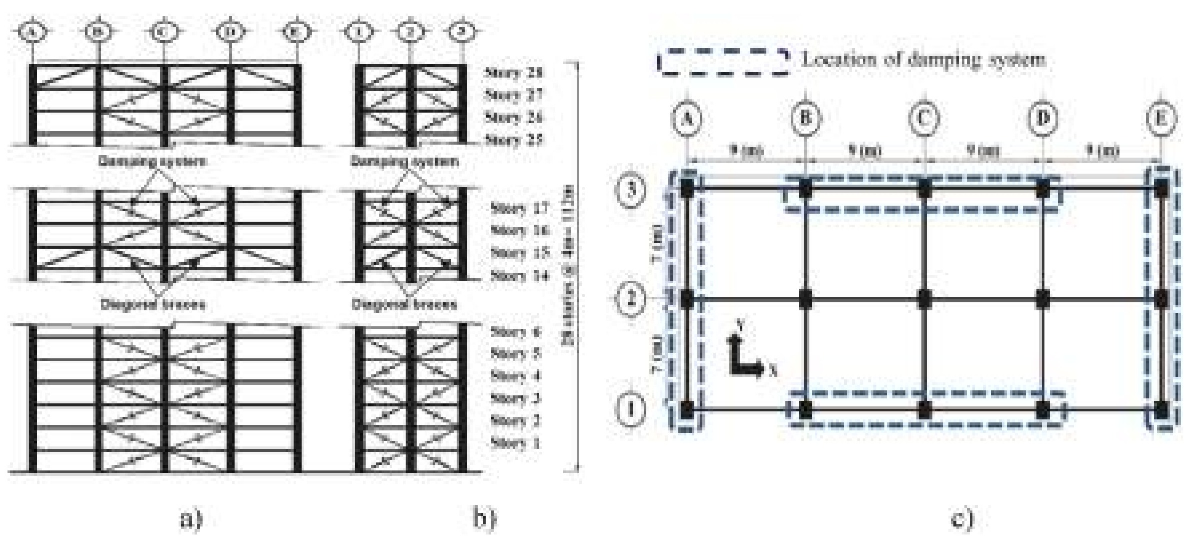

Fig. 1. Configuration of the building structure: a) elevation view in X-direction (longitudinal); b) elevation view in Y-direction (transversal); and c) location of the damping system.

Table 1
Columns for the conventional building (left) and with damping system (right).

Section	Stories	f'c (kg/cm^2)	E_c (kg/cm^2)	Section	Stories	f'c (kg/cm^2)	E_c (kg/cm^2)
C1 (1.10x1.25)$^{2.8\ \%}$	PB-N3	500	288885	C1 (0.90x1.10)$^{3.6\ \%}$	PB-N5	500	288885
C1 (1.10x1.25)$^{1.0\ \%}$	N3–N12			C1 (0.90x1.00)$^{1.6\ \%}$	N5–N10		
C2 (0.95x1.10)$^{1.0\ \%}$	N12–N18			C2 (0.90x0.90)$^{1.7\ \%}$	N10–N15		
C3 (0.90x1.05)$^{1.0\ \%}$	N18–N25			C3 (0.80x0.90)$^{2.0\ \%}$	N15–N20		
C6 (0.70x0.70)$^{1.0\ \%}$	N25–N28	350	261916	C6 (0.70x0.70)$^{1.0\ \%}$	N20–N28	350	261916

Table 2
Beams (X direction) for the conventional building (left) and with damping system (right).

Section	Stories	fy (kg/cm^2)	E_s (kg/cm^2)	Section	Stories	Fy (kg/cm^2)	E_s (kg/cm^2)
W30x116	N1–N8	3515	2039000	W30x90	N1–N6	3515	2039000
W30x99	N9–N13			W27x84	N7–N14		
W27x84	N14			W24x76	N15–N26		
W24x76	N15–N17			W27x84	N26–N28		
W27x84	N18–N23						
W24x76	N24–N26						
W27x84	N27–N28						

Table 3
Beams (Y direction) for the conventional building (left) and with damping system (right).

Section	Stories	fy (kg/cm^2)	E_s (kg/cm^2)	Section	Stories	Fy (kg/cm^2)	E_s (kg/cm^2)
W33x130	N1–N13	3515	2039000	W30x99	N1–N2	3515	2039000
W30X99	N14–N15			W30x108	N3–N7		
W30x116	N15–N23			W30x99	N8–N19		
W30X99	N24–N26			W27x84	N20–N23		
W24X76	N27–N28			W24x76	N24–N28		

Table 4
Outrigger system for the conventional building (left) and with damping system (right).

Section	Stories	fy (kg/cm^2)	E_s (kg/cm^2)	Section	Stories	Fy (kg/cm^2)	E_s (kg/cm^2)
W12x96	N14-15	3515	2039000	W12x96	N14-15	3515	2039000
W12x96	N27-28			W12x96	N27-28		

Table 5
Properties of the dampers for the buildings with damping system.

Case study	Damping exponent, α	Damping constant, C (ton (s/m) $^{\alpha}$)	Case study	Damping exponent, α	Damping constant, C (ton (s/m) $^{\alpha}$)
E−01	0.1	150	E−06	0.6	696
E−02	0.2	207	E−07	0.7	925
E−03	0.3	284	E−08	0.8	1221
E−04	0.4	386	E−09	0.9	1595
E−05	0.5	520	E−10	1.0	2070

indicating the percentage of steel in the columns is also included. The Phase 1 has been finished, which involved designing a group of 28-story buildings that are equipped with viscous fluid dampers.

5. Phase 2: seismic performance assessment of the case studies

5.1. Performance model for the case studies (step 1)

During Phase 2, the main objective is to assess the seismic performance of the case studies, using the FEMA P-58 methodology [15]. Accordingly, this approach consists of multiple steps. The first step involves constructing the performance model, which implies gathering data related to the size of the structure, replacement quantities, intended use and, fundamentally, the identification of the building components and their vulnerability. This requires establishing the plan and elevation dimensions of the structure, as shown in Fig. 1. Additionally, it is important to define the total replacement cost, which requires a detailed quantification of its components. For the case studies, the costs of structural elements, connections, fabrication and assembly, electrical and plumbing installations, tempered facade glass, and waste, among others, were included in the total replacement cost. Moreover, the total replacement cost should also include: the costs associated with demolishing and removing debris from the site, in case of a collapse of the structure. According to FEMA P-58 [15], demolition and waste removal can increase the total replacement cost by approximately 20 %–30 %. Therefore, a 25 % increase in the total replacement cost was utilized in the present study to account for those costs.

Furthermore, in addition to determining the total replacement cost of the building, it is also important to establish replacement quantities in terms of environmental impact. To achieve this, a database developed by Yang et al. [70] was used, which provides various environmental impact factors related to structure construction for different building occupancies (*e.g.*, commercial office, healthcare, hospitality, etc.). According to the database, constructing a hotel generates a specific amount of carbon emissions and embodied energy per US dollar spent of 0.326 kg CO2eq/US$ and 5.791 MJ/US$, respectively. It should be noted that this database corresponds to the United States economy in 2013. Therefore, taking into account inflation and the change in the value of the dollar between June 2013 and January 2023 (which is 1.28 according to the U. S. Bureau of Labor Statistics [81]), the amounts of carbon emissions and embodied energy for January 2023 are 0.254 kg CO2eq/US$ and 4.524 MJ/US$, respectively. Subsequently, these environmental impact factors are multiplied by the total replacement cost of the building to obtain the replacement amounts associated with carbon emissions and embodied energy for the case studies.

Constructing the performance model also requires specifying the building occupancy, as this information is useful to establish a model that represents the distribution of people inside the structure at different times of the day. This is important for assessing the potential for injuries and fatalities when the building is occupied. As mentioned earlier, the building is intended for hospitality use. In this sense, Seligson [82] provides population models related to different occupation purposes and one of them adapts well to the case study. Fig. 2 shows the selected model, which defines the number of people inside the building on weekdays and weekends as a function of the time of day. The model establishes a maximum value of 2.5 people per approximately 100 square meters and has a dispersion of 0.2.

Likewise, specifying the occupational use of the structure facilitates estimating the quantity of non-structural components and contents that are in the building (windows, partition walls, ceilings, elevators, HVAC-related pipes, etc.). In this regard, the FEMA P-58 methodology presents a study of approximately 3000 buildings with different occupational uses. The results of this study were translated into a tool that gives the average quantities of non-structural components and contents in a structure based on its occupancy. Hence, in this study, this tool we utilized to estimate the aforementioned components [66].

Determining the vulnerability of both structural and non-structural elements in the building is also necessary for constructing the performance model. Vulnerability is determined using fragility curves, which quantify the likelihood of an element being damaged at a particular structural demand parameter [83]. The PACT database [66] provides a repertoire of fragility curves for various structural and non-structural elements, along with the associated consequences at different levels of damage states that can be generated in terms of repair costs, repair time, and environmental impact. These curves were developed based on experimental test data [84,85].

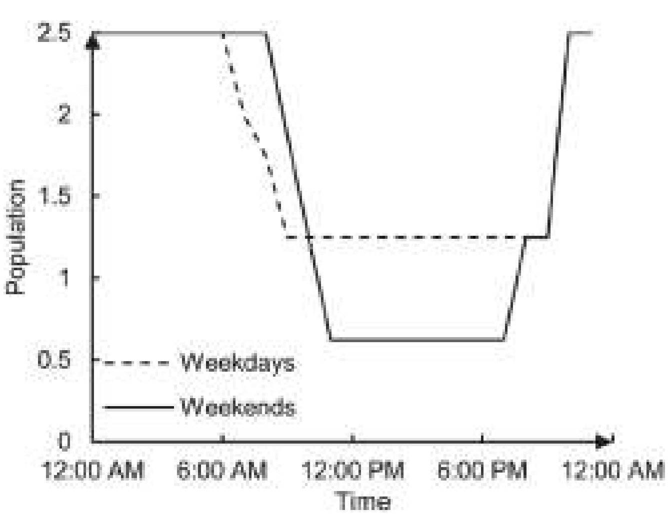

Fig. 2. Variation in the number of people in the building (related to the expected peak population) as a function of time of day for hospitality occupancy.

In cases where there is no information available regarding the fragility of building components, FEMA P-58 recommends a set of protocols for testing the behavior of both structural and non-structural elements experimentally and determining their vulnerability using fragility curves [15,86]. For the case studies conducted in this research, fragility functions from the PACT database [66] were utilized. These functions were chosen because of their experimental derivation and probabilistic nature, which consider factors such as construction techniques, material quality, and other variables that can affect the vulnerability of both structural and non-structural elements. The dispersion contained in the fragility functions accounts for the fact that the tested specimens may not have been built using local construction techniques and materials. Hence, the available data is a good approximation for characterizing the vulnerability of the components in the case studies.

In this context, fragility curves for viscous dampers were not available in the PACT database. In this study, to consider the consequences of failure of the damping devices, similar to Santos-Santiago et al. [33], it was proposed using two different failure modes: 1) related to the force-velocity levels that the devices can experience, and 2) associated with the maximum relative displacement between their extremes. Therefore, two analytical fragility curves were determined. The model representing damping device failure considers the following:

- The model proposed by Miyamoto et al. [87] was used to determine the maximum force that the viscous damper can generate.
- The maximum force that indicates the onset of the damping device failure is associated with an over-velocity condition, as outlined in Section 7.3.2 of the European code for anti-seismic devices (EN 15129) [52].
- The maximum displacement that the damper develops before failure in tension is when the piston extension reaches the stroke limit. In this study, a stroke limit of $\pm$40 mm was considered.
- The viscous damper does not fail as long as the displacements, velocities, and forces of the damper remain lower than those obtained when subjected to the design seismic intensity.
- It is assumed that the steel diagonal brace connecting the viscous damper to the structural system exhibits linear behavior and can withstand the maximum forces that the damper can develop.
- In this study, only one damage state was considered, specifically the damage or failure of the viscous devices. In this context, the financial consequences are associated with the replacement cost of the damper. The replacement cost includes expenses related to manufacturing, transportation, and device import. Additionally, a sensitivity analysis was conducted to include the environmental consequences based on those observed for steel braces within PACT database. Moreover, as observed for same fragility specifications, potential for non-collapse casualties were not included.

Fig. 3a and b displays the hysteresis loops (force-displacement) of specific viscous dampers located in the lower stories of the analyzed structures. The response corresponds to different ground motions (refer to Table 6) scaled to a seismic intensity of 0.5g with selected values of α. As expected, the figures demonstrate that the damping devices generate significant forces and undergo failure when the piston's extension reaches the stroke limit (*i.e.*, $\pm$40 mm).

The consequence functions related to repair costs were developed in 2011 for the northern region of California, United States (U.S.). Hence, it is reasonable to assume that these costs need adjustment to the specific geographical location of the structure, as well as the current economic conditions. To address the issue of inflation, the change in the value of the dollar between June 2011 to January 2023 is 1.33, according to data reported by the U.S. Bureau of Labor Statistics [81]. To adjust the repair costs from the PACT database [66] to the local situation, the following approximation was utilized [88,89]:

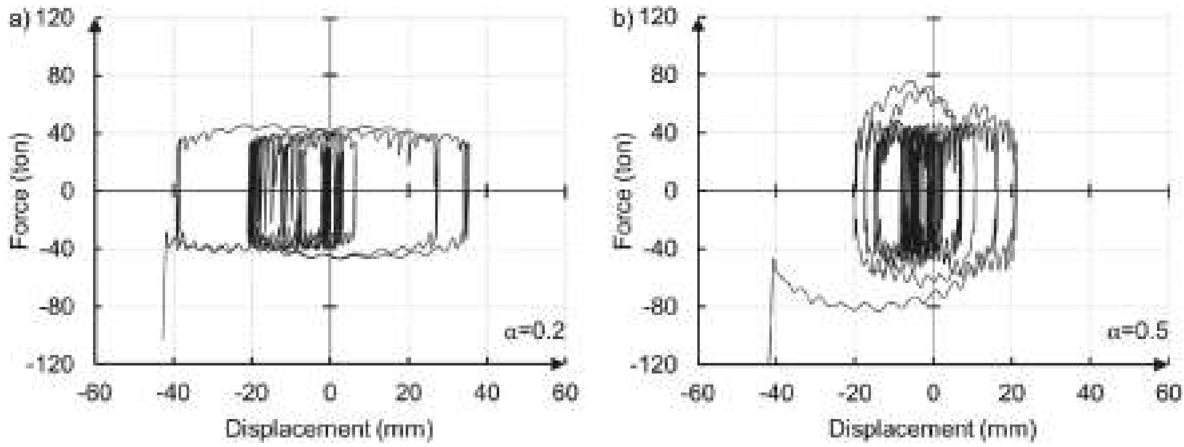

Fig. 3. Hysteretic behavior of viscous dampers showing damping device failure due to excessive displacement.

Table 6
Ground motion records for the nonlinear time-history analyses.

Name	Station	Date	Latitude	Longitude	M_w	Depth
EQ-01	COYC	14/09/1995	16.31	98.88	7.2	22
EQ-02	COYC	11/01/1997	17.91	103.04	6.9	16
EQ-03	COYC	15/06/1999	18.18	97.51	6.5	69
EQ-04	COYC	30/09/1999	15.95	97.03	7.1	17
EQ-05	COYC	12/12/2011	17.84	99.98	6.5	58
EQ-06	ACAD	14/09/1995	16.31	98.88	7.2	22
EQ-07	ACAC	14/09/1995	16.31	98.88	7.2	22
EQ-08	ACAD	14/09/1995	16.31	98.88	7.2	22
EQ-09	ACAD	11/01/1997	17.91	103.04	6.9	16
EQ-10	ACAD	15/06/1999	18.18	97.51	6.5	69
EQ-11	ACAD	30/09/1999	15.95	97.03	7.1	17
EQ-12	ACAD	11/12/2011	17.84	99.98	6.5	58

$$C^{i}_{\ local\ cost} = C^{i}_{\ US\ cost}[(1 - f_{lab}).r_{mat} + f_{lab}.r_{lab}] \tag{3}$$

where $C^i_{local\ cost}$ refers to the mean unit repair cost in the local area, while $C^i_{US\ cost}$ is the mean unit repair cost in the U.S. On the other hand, f_{lab} denotes the fraction of the unit repair cost in the U.S. associated with labor. Porter et al. [88] recommends using a value of 0.9 when repairing architectural, structural, and mechanical, electrical, and plumbing systems if more precise information is not available. A value of 0.5 is recommended for actions involving the replacement of architectural and structural components, and a value of 0.1 is suggested for the replacement of mechanical, electrical, and plumbing equipment. These values are determined based on the significance of the materials and labor costs involved in the repair process. Additionally, the parameters r_{mat} and r_{lab} represent the ratios between the local cost of materials and labor compared to their costs in the U.S. These parameters are established using a report by Turner and Townsend [90] that compares construction costs in various cities around the world. For this research, San Francisco (California) and Mexico City are used as benchmark cities. San Francisco was chosen due to its status as the most expensive place to build (per square meter) in the United States, and Mexico City was selected because it was the sole Mexican city included in the report.

5.2. Characterization of seismic hazard and ground motions selection (step 2)

The FEMA P-58 methodology [15] proposes three techniques for assessing the performance of structures: intensity-based, scenario-based, and time-based. The intensity-based method assesses the expected performance of the structure when exposed to a specific seismic intensity, while the scenario-based approach evaluates the performance of the structure during a seismic event with a particular magnitude and distance. On the other hand, the time-based approach estimates the probable performance of the structure over a specified period of time, considering the probability of occurrence of all seismic events that could happen during that time. This approach also includes the uncertainty related to the magnitude, distance, and intensity of possible seismic events. To conduct a time-based seismic performance evaluation, it is necessary to carry out a probabilistic seismic hazard analysis.

A time-based analysis was performed in the study, as shown in Fig. 4, which depicts the mean annual rate of exceedance of $Sa(T_1)$ corresponding to the site of interest (Acapulco, Guerrero, Mexico) [91], and the fundamental period of the building (*i.e.*, hazard curve). The curve is divided into ten equal $Sa(T_1)$ intervals represented by triangular markers. In addition, the exceedance rate associated with the intensity at the midpoint of each interval is identified by circles.

Then, the performance is evaluated using the intensity-based method for each interval of the seismic hazard curve (triangles), where the target intensity corresponds to the mean value of each interval (circles). The computed performance data were then weighted by the exceedance rate corresponding to each target intensity. The results of these evaluations are summed up for each interval to obtain the mean annual rate of exceedance of a performance measure.

Furthermore, this stage involved collecting accelerograms from earthquake events recorded on firm ground near the site of interest: Acapulco, Guerrero, Mexico. According to the Mexican seismic design guidelines [2], when using the nonlinear time-history method, eight to twelve representative pairs of ground motions should be chosen based

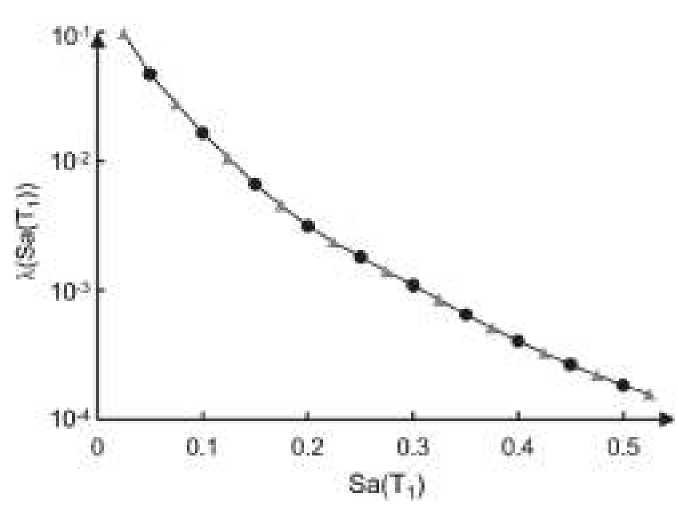

Fig. 4. Mean annual rate of exceedance (λ) of $Sa(T_1)$ for the site of reference, associated to the fundamental period of the structure $T_1 = 4.7$s.

on dynamic soil conditions. These guidelines also suggest conducting a probabilistic seismic hazard analysis and a deaggregation process to identify the most probable combination of magnitude, source-to-site distance, and focal mechanism associated with a specific intensity [92], serving as the criterion for ground motion selection.

However, due to limited availability of ground motion data in the region, selecting ground motions based on specific characteristics is not feasible, nor is a formal ground motion selection procedure accessible (*e.g.* Ref. [93]). Instead, ground motion records associated with moment magnitudes (M_w) equal to or greater than 6.5 and epicentral distances of approximately 30 km were chosen. This decision was based on our observation that ground motions related to moment magnitudes below 6.5 and distances greater than 30 km did not produce significant seismic responses in our case studies; moreover, incremental dynamic analyses required significant scaling factors to induce nonlinear responses. Additionally, it was verified that the records had a similar spectral shape. This ensures scaling the ground motion records during subsequent nonlinear analyses from introducing bias in the nonlinear displacement estimates, preventing an overestimation of structural collapse probabilities.

Concerning the focal mechanism, the port of Acapulco, Guerrero, experiences both interplate and intraslab seismic events. Interplate earthquakes occur along the Cocos-North American plate boundary, specifically along Mexico's Pacific coastline. These earthquakes involve rupture along a low-angle thrust plane at shallow depths of approximately 15–25 km [94]. Intraslab earthquakes, on the other hand, occur within the subducted Cocos plate, typically at depths of 40–80 km beneath the center of the country, and involve normal faulting. In addition, steeply dipping thrust seismic events near the coast can also be categorized as normal-faulting intraslab earthquakes due to the similarity of their ground motions [95,96].

Therefore, in this study, twelve pairs of ground-motion records associated with interplate and intraslab earthquakes were utilized, categorized based on their focal mechanisms. Records corresponding to depths less than 40 km were classified as interplate, while those with depths equal to or greater than 40 km were categorized as intraslab, following the classification criteria by Singh et al. [96]. The selected ground motion records were then used to perform subsequent nonlinear time-history analyses for the case studies. The Strong Motion Network of the Institute of Engineering at UNAM, Mexico (RAII-UNAM), provided the ground motions, which correspond to seismic events with moment magnitudes (M_w) equal to or greater than 6.5, and epicentral distances of around 30 km (Table 6).

All records underwent linear baseline correction and bandpass filter

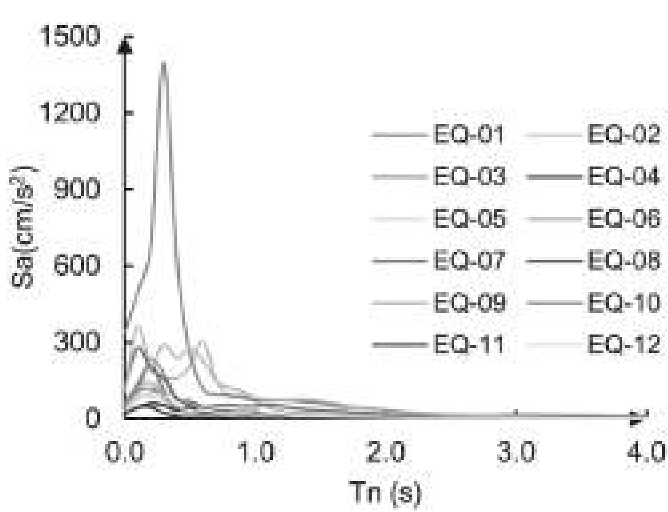

Fig. 5. Pseudo-acceleration response spectra associated with the ground motions records indicated in Table 6.

with corner frequencies of 0.1 and 25 Hz. The duration of the ground motions was also adjusted to correspond to a range between 5 % and 95 % of the Arias intensity. Fig. 5 shows the pseudo-acceleration response spectra for the compiled seismic records.

On the other hand, scaling factors were used to modify the selected accelerograms and achieve the desired intensity level when calculating the spectral acceleration response spectra. This is a common practice when performing nonlinear time-history analyses [97]. In this sense, the seismic records were scaled using Sa_{avg} intensity measure [98], which is known for its ability to predict the seismic demand of nonlinear structural systems, particularly those that exhibit both influence of their higher modes and degrading behavior [99–103]. The expression for Sa_{avg} is as follows:

$$Sa_{avg}(T_1 \dots T_N) = \left(\prod_{i=1}^{N} Sa(T_i) \right)^{1/N} \tag{4}$$

where Sa_{avg} is the geometric mean of spectral acceleration values, associated with N number of vibration periods, within an interval defined by an initial period T_1 and a final period T_N. According to the Mexican seismic design guidelines [2], in this study, T_1 corresponds to 0.2 times the fundamental period of the structure ($T_1 = 0.2T_e$), while T_N is 1.5 times vibration period ($T_N = 1.5T_e$).

5.3. Nonlinear response for the case studies (step 3)

In this study, a time-history analysis is employed to determine the structural response, which is a fundamental step in performance evaluation. Although the structural designs established in Phase 1 have been useful in defining building sections, the non-linear response of the case studies (*i.e.*, E−00 to E−10) was obtained using the Ruaumoko 3D program [104]. This program enables systematic multiple nonlinear analyses of a structure subjected to various ground motion records.

The beams and columns of the building were modeled as frame elements with concentrated plastic hinges in order to characterize their non-linear behavior. To achieve this, the Ramberg-Osgood and the modified Takeda hysteresis models were employed for beams and columns, respectively [105,106]. The viscous damping devices were modeled as damper type elements and the damping constant C and exponent α were determined according to the simplified modal-based method (see Table 5).

A damping ratio of 2 % was assumed for all modes that influence the building response using the Rayleigh damping model. Additionally, second-order effects (P-Δ) were also included. To simplify the analyses, a rigid foundation was considered at the base of the building, since soil-structure interaction effects were not accounted. This was based on the assumption that the structure was on a firm-ground site. The soil classification was identified as Type I, denoting a firm ground or rock site with an average shear wave velocity ≥750 m/s, in accordance with the soil classification criteria outlined in the Manual for Civil Structures Design by CFE [55]. This site classification falls within the range of Site Class B and Site Class C, as defined by the American Society of Civil Engineers document (ASCE/SEI 7–16) [1].

The purpose at this stage is to obtain the nonlinear response for the case studies (*i.e.*, E−00 to E−10). As already mentioned, the buildings were modeled using Ruaumoko 3D software [104], and were subjected to 12 pairs of accelerograms (Table 6) scaled for different intensity levels as described in the preceding section. The objective of these analyses was to determine the interstory drifts and floor accelerations. Fig. 6 shows the maximum interstory drifts obtained for each floor of the E−06 structure (*i.e.*, $\alpha = 0.6$) in the E-W direction.

These results were obtained by subjecting the building to the compiled seismic records (Fig. 5) scaled to an intensity of 0.50g (associated with the last circle in Fig. 4). The maximum interstory drifts and floor accelerations were calculated for both the N–S and E-O orthogonal components, for each of the intensity values indicated in the seismic

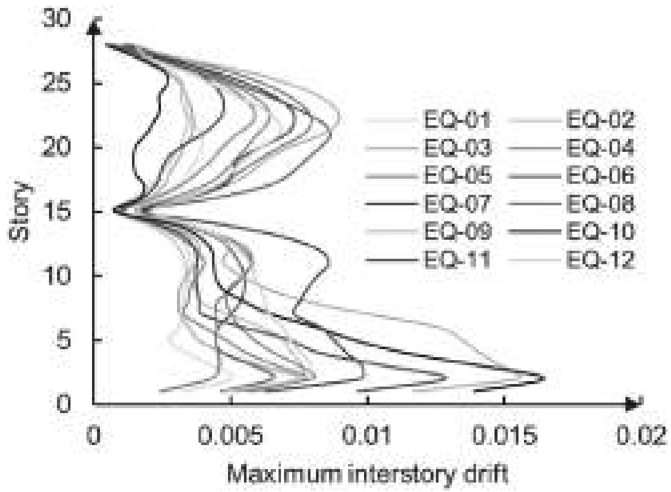

Fig. 6. Maximum interstory drift for the case study E−06 (*i.e.*, $\alpha = 0.6$) resulting from the seismic records scaled to an intensity level of 0.50g.

hazard curve (circles in Fig. 4), and for all case studies (E−00 to E−10). It is worth noting that the significant reduction in interstory drifts can be attributed to the inclusion of the diagonal brace system on stories 15 and 28.

Fig. 6 provides a graphical representation of the results. However, what is needed is to assemble a demand parameter matrix. In this matrix, the columns are associated with demand vectors belonging to story level of the building, and the row vectors are related to the response that each seismic record produces. This matrix serves as a seed for generating a set of simulated demands are then used to compute the performance. Hence, Table 7 illustrates the structure of this matrix.

5.4. *Incremental dynamic analyses (IDAs) and collapse fragility curve (step 4)*

The preceding section aimed to determine the seismic response of a building at a specific intensity level through nonlinear analyses, which enabled to assemble a demand parameter matrix employed to generate a set of simulated demands to evaluate the performance. Nonlinear analyses also facilitate the implementation of IDAs (Incremental Dynamic Analyses) as described by Vamvatsikos and Cornell [65]. By using the results of these type of analyses, it is possible to establish the collapse fragility curve, which allows the assessment of performance based on the number of injuries and fatalities.

The following results were obtained from a sequence of IDAs. The accelerograms used in the analyses were scaled to generate intensity levels ranging from 0.05g to 2.0g (with 0.05g intervals). Fig. 7a and b illustrate the IDA outcomes for the E−04 and E−08 case studies, respectively. The solid lines in the figures represent the response, in terms of the maximum interstory drift experienced on any of the story levels, obtained for each of the scaled accelerograms until the collapse of the structure is produced. In this research, it is assumed that the collapse of the structure occurs when a) intensity levels greater than 2g are reached; b) a convergence error is produced (generating excessive response values); and/or c) the slope of the tangent line of the curve is less than or equal to 20 % of the elastic slope [65].

On the other hand, the dashed line corresponds to the average of the predicted response for each of the seismic records, which can be interpreted as a type of capacity curve. In general, all curves exhibit an elastic region that ends once the first plastic hinge appears. Following the first nonlinear incursion, some curves show a *softening* of the system, which results in displacements increasing rapidly until the collapse of the structure occurs. Similarly, there are curves that display successive patterns of *softening* and *hardening*. However, collapse of the building is eventually generated.

Based on the obtained results, it is possible to identify the number of collapses that occur for each intensity level. Therefore, the collapse probability given a certain intensity level, $P(C|IM)$, can be calculated as follows:

$$P(C|IM) = \frac{n}{N} \tag{5}$$

where n is the number of analyses that result in the collapse of the structure for a specific intensity level, while and N refers to the total number of analyses conducted for that intensity. Fig. 8a and b presents the $P(C|IM)$ values for case studies E−04 and E−08, respectively (dots). A distribution function (continuous line) has been fitted to these values. As a result, the probability of collapse is expressed using a lognormal distribution function of IM. In this study, the collapse fragility curve was established using the Collapse Fragility Tool provided by FEMA P-58 [66].

For case E−04, a mean value of $\theta = 1.3$g and a standard deviation $\beta = 0.227$ were obtained. For case E−08, a mean value of $\theta = 0.81$g and a standard deviation $\beta = 0.291$ were determined. This implies that, on average, there is a 50 % of collapse probability when an intensity level of 1.3g and 0.81g is reached for case E−04 and E−08, respectively. In other words, under the specified conditions in these case studies, the structure with a damping system where the exponent $\boldsymbol{\alpha}$ equals 0.8 is more susceptible to collapse than the system where $\boldsymbol{\alpha}$ equals 0.4.

Table 7
Example of an EDP matrix for different seismic records (E−06, intensity of 0.50g).

Seismic record	*EDP* 1	*EDP* 2	*EDP* 3	*EDP* 4	…	*EDP* 28
EQ-01	0.0032	0.0050	0.0043	0.0033	…	0.0007
EQ-02	0.0048	0.0075	0.0076	0.0072	…	0.0005
EQ-03	0.0058	0.0075	0.0060	0.0047	…	0.0007
.	.	.	.	.	.	.
.	.	.	.	.	.	.
.	.	.	.	.	.	.
EQ-12	0.0047	0.0075	0.0079	0.0075	…	0.0015

5.5. *Performance evaluation for the case studies (step 5)*

The FEMA P-58 methodology [15] employs the Monte Carlo method and a matrix of simulated demands obtained from limited nonlinear analyses to account for uncertainties in seismic performance evaluation. These simulated demand vectors, known as “realizations”, contain values of structural demand for each level and direction of analysis in the building, and their number can range from hundreds to thousands.

Fig. 9 provides a flowchart to facilitate understanding of the performance evaluation process (adapted from Ref. [15]).

The performance calculation begins with the first realization, which determines whether the structure collapses based on a random number and the collapse fragility curve. If collapse occurs, replacement values are used to calculate losses, determine the number of injuries and deaths based on building occupancy, and classify the structure as unsafe due to instability. Another realization is then carried out.

If collapse does not occur, the level of damage generated by the seismic action is evaluated to determine if it is reparable based on maximum residual drift ratios and a fragility curve associated with the feasibility to repair the building. If the structure is deemed irreparable, it is classified as unsafe, and losses are calculated using replacement values, along with the number of injuries and deaths. Another realization is then performed. The FEMA P-58 methodology offers simplified equations for calculating median residual drift ratios based on the peak transient response of the structure [15]. However, Alehojjat et al. [107] conducted a study to assess the accuracy of three approximate methods, including the FEMA P-58 approach [15], in estimating residual

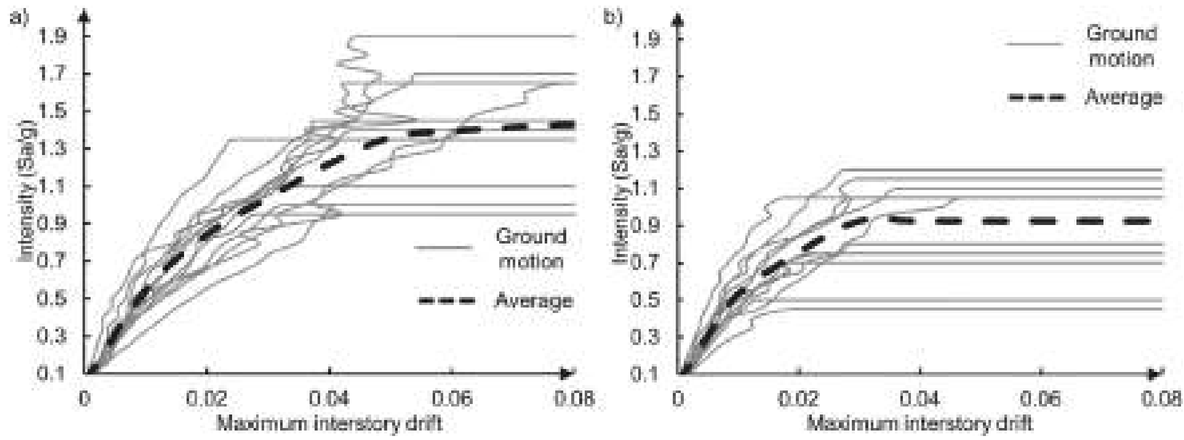

Fig. 7. Incremental Dynamic analyses related to the ground motion records of Table 6: a) case E−04 and b) case E−08.

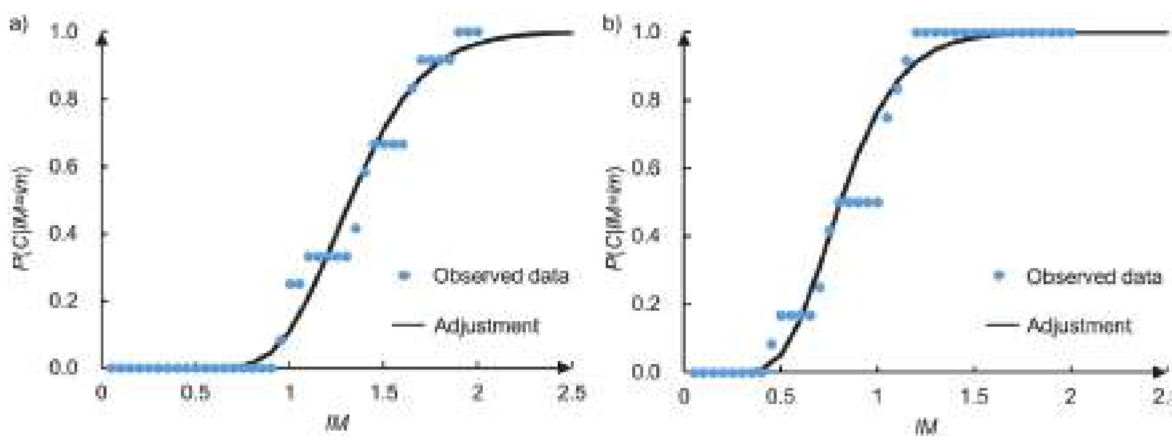

Fig. 8. Fragility curves associated to the collapse of the building: a) case E−04, and b) case E−08.

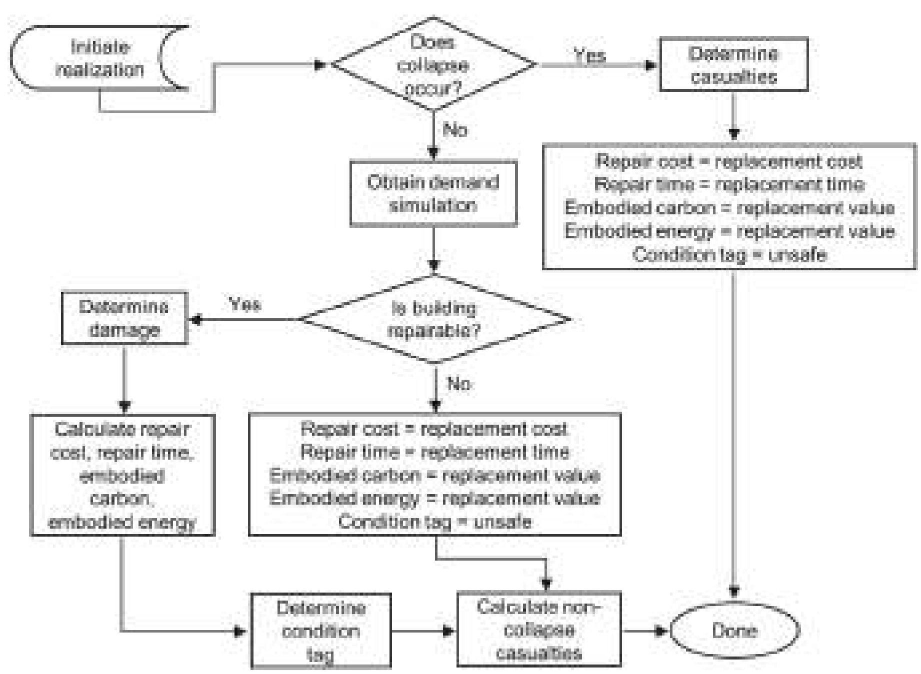

Fig. 9. Flowchart for assessing a performance outcome in each realization, adapted from Ref. [15].

interstory drift ratio demands in mid-rise steel structures equipped with fluid viscous dampers; they concluded that FEMA P-58 [15] method overestimated residual interstory drift ratio demands at the design earthquake hazard level but underestimated them at the maximum considered earthquake hazard level. Consequently, in this study, the residual drift ratios obtained from nonlinear time history analyses were utilized instead.

If the remaining damage is reparable, the fragility functions of the structural and non-structural elements are used to assign a random damage state and calculate losses accordingly. The sum of losses for each component gives the total loss for that realization. This process is repeated for all realizations, and the resulting loss values are sorted in ascending order to obtain the distribution function of the decision variable of interest. As this procedure is highly repetitive, the electronic tool PACT [66] was utilized in this study to carry out probabilistic and loss accumulation calculations using its collection of fragility and consequence functions.

5.5.1. *Performance functions for the case studies*

The precise calculation of the seismic performance of a building cannot be done due to the inherent uncertainties involved in the process. However, it is possible to define the probability that the performance variable is less than or equal to a specific value as a result of a particular level of seismic intensity. Fig. 10a–d presents various performance curves in terms of repair costs associated to different levels of seismic intensity and case studies. It is important to point out that the repair costs were normalized with respect to the total cost of replacement of the structure, which gives a more intuitive understanding of the consequences of the damage produced.

The distribution functions shown in Fig. 10a correspond to the "conventional building" structure, with no viscous damping devices (E−00). In this regard, if the objective is to determine the average repair costs for intensity levels ranging from 0.1g to 0.2g (*i.e.*, associated with a 50 % probability of non-exceedance), the estimated costs would be around 2.5 % of the total replacement cost of the building. Similarly, for the same intensity levels but associated with a 90 % probability of non-exceedance, which implies a higher degree of certainty, the average repair costs would be approximately 5 % of the total replacement cost of the structure. This suggests that if a seismic event of this intensity were to occur, the maximum probable cost would be 5 % of the total cost for these intensity levels (*i.e.*, 0.1g and 0.2g). Conversely, the repair costs associated with a 90 % probability of non-exceedance for intensity levels ranging from 0.4g and 0.5g would be approximately 25 % and 60 % of the cost of the structure, respectively.

The inclusion of energy dissipation devices is recommended to enhance building performance, as mentioned earlier. Fig. 10d illustrates the results obtained for structure E−10, which includes a linear viscous damping system ($\alpha = 1.0$). The results indicate that for seismic intensities of 0.4g and 0.5g, the repair costs related to a 90 % probability of non-exceedance are around 25 % and 50 % of the building total cost, respectively. These results demonstrate an improvement in performance of 10 % compared to the E−00 case but only for a seismic intensity of 0.5g. On the other hand, Fig. 10c shows the performance results of structure E−05 ($\alpha = 0.5$). In this case, utilizing the same analysis condition as E−10, the repair costs are estimated to be roughly 10 % and 25 % of the total cost of the building, respectively. This suggests that E−05

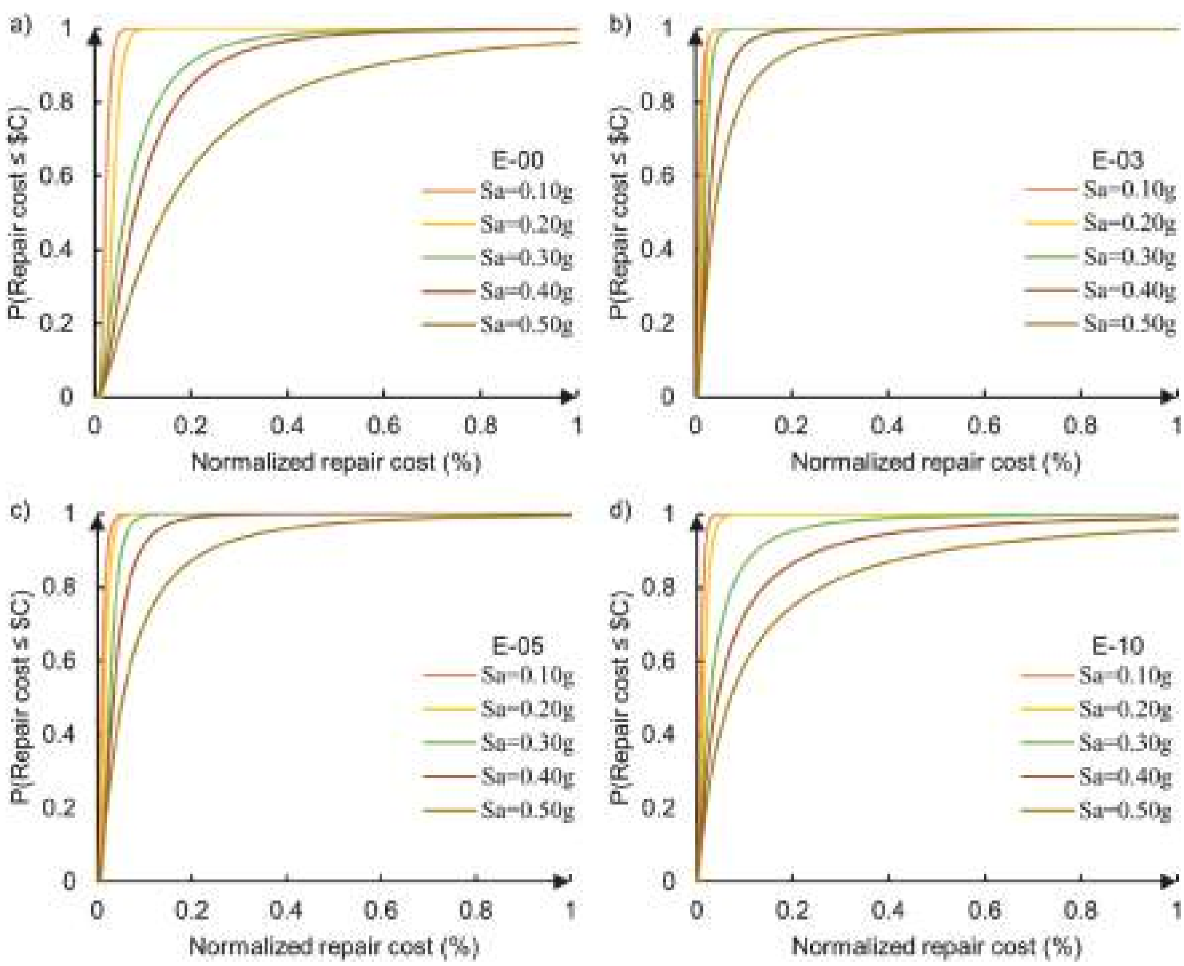

Fig. 10. Performance functions in terms of normalized repair costs for different levels of seismic intensity and case studies.

outperforms the two previous case studies (*i.e.*, E−00 and E−10). Lastly, referring to Fig. 10b, under identical analysis conditions, the repair costs are nearly 7.5 % and 15 % of the cost of replacing the structure. Hence, structure E−03 ($\alpha = 0.3$) exhibits superior performance compared to the three prior case studies (*i.e.*, E−00, E−05, and E−10).

Additionally, the assessment of building performance is also expressed in terms of its environmental impact, specifically its equivalent carbon dioxide emissions (kg-CO_2eq) and the number of injuries. In this regard, Fig. 11a and b depict the performance functions that represent carbon dioxide emissions resulting from repair actions to restore the building to its initial condition. These performance functions correspond to various seismic intensity levels and two specific case studies (E−00 and E−03). It should be noted that the carbon dioxide emissions are normalized based on the total carbon dioxide produced during the construction stage of the building.

It is possible to conduct an analysis similar to the one described earlier. However, for the sake of brevity, some specific observations are made. For instance, Fig. 11a shows the case study where damping devices (E−00) are not implemented. It indicates that the environmental impact for intensities of 0.4g and 0.5g, with a 90 % probability of non-exceedance, is respectively 50 % and 80 % of the carbon dioxide emissions emitted during the construction phase. On the other hand, the incorporation of energy dissipation devices (Fig. 11b) reduces the environmental impact resulting from repair actions to approximately 25 % and 35 % for the same intensity levels, respectively. If this information is related to that obtained for the case where repair costs were evaluated (Fig. 10b), it can be established that the repair costs for intensities of 0.4g and 0.5g, considering a 90 % probability of non-exceedance, are approximately 7.5 % and 15 % of the total replacement cost. Correspondingly, those repair actions would generate an environmental impact close to 25 % and 35 % of the carbon dioxide emissions emitted during the construction phase, respectively.

Fig. 12a and b presents the performance functions in terms of the number of injuries. In Fig. 12a, which represents the case study without damping devices, the analysis shows that for intensities of 0.4g and 0.5g with a 90 % probability of non-exceedance, the number of people injured is 5 and 15, respectively. On the other hand, the implementation of viscous damping devices, as shown in Fig. 12b, reduces the number of injuries to less than 5 people for both intensities.

5.5.2. *Probability of exceedance of performance measures and expected annual losses*

In the preceding section, the distribution functions were derived by utilizing the intensity-based method to assess performance. While these performance curves provide valuable insights for a specific seismic intensity level, they do not consider the probability of occurrence of such intensity levels. To address this, a time-based evaluation is necessary. This approach takes the performance results from the intensity-based method (Figs. 10–12) and weights them with respect to the probability of exceedance of each analyzed intensity (circles in Fig. 4). The results of these evaluations are then summed for each intensity, and the outcome is expressed as the mean annual rate of exceedance for a particular performance measure. The following equation represents this process mathematically (all variables involved have been previously defined):

$$P(DV > dv) = \int_{\lambda} P(DV > dv | IM = im) d\lambda(IM) \tag{6}$$

Figs. 13–15 present the mean annual rate of exceedance associated with repair costs (normalized), environmental impact (normalized), and the number of people injured, respectively. These results correspond to the case studies E−00 (Figs. 13a, 14a and 15a) and E−05 (Figs. 13b, 14b and 15b). Additionally, the contribution of every intensity level (represented by circles in Fig. 4) to the total exceedance rate (envelope) is also included.

The analysis above indicates that low seismic intensity levels make the most significant contribution to the total exceedance rate, particularly in terms of repair costs (Fig. 13) and environmental impact (Fig. 14). Conversely, higher intensity values have a lower impact on the total exceedance rate. This can be attributed to the reduction in the derivative of the seismic hazard curve ($d\lambda(IM)$ in equation 10) as seismic intensity values increase (represented by circles in Fig. 4), resulting in a smaller contribution. Fig. 15a, which illustrates the number of injured, exhibits a similar trend. However, for structure E−05 (Fig. 15b), intensity levels ranging from 0.05g to 0.20g do not contribute to the number of injuries, as these intensity levels generate zero losses in terms of injuries.

As anticipated, the probability of exceeding a certain performance value, such as repair costs, environmental impact, and the number of injuries, is higher for the structure without an energy dissipation system (E−00), in comparison to the structures equipped with a damping system (E−01 to E−10).

6. Optimal sustainable design based on expected annual losses

While Figs. 13–15 enable the identification of the probability of exceeding a particular performance value and comparison of results between the two study cases (*i.e.*, with and without damping system), a comprehensive comparison scenario is possible through the expected annual loss (EAL). The EAL corresponds to the area under the curve of the mean annual rate of exceedance and represents the total loss that is expected to occur within a year. It is a useful measure in determining

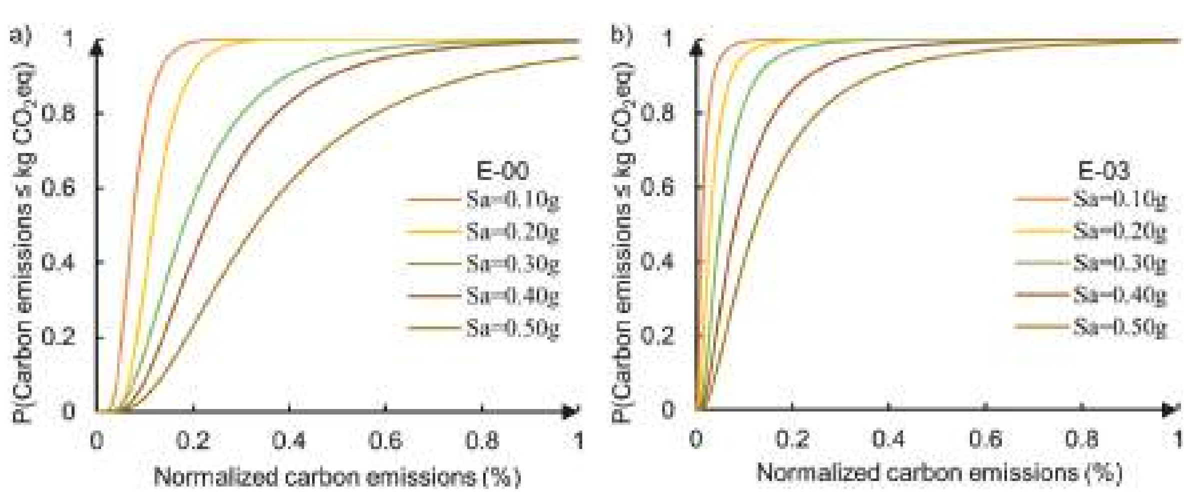

Fig. 11. Performance functions in terms of normalized carbon emissions (environmental impact) for different levels of seismic intensity and for two case studies.

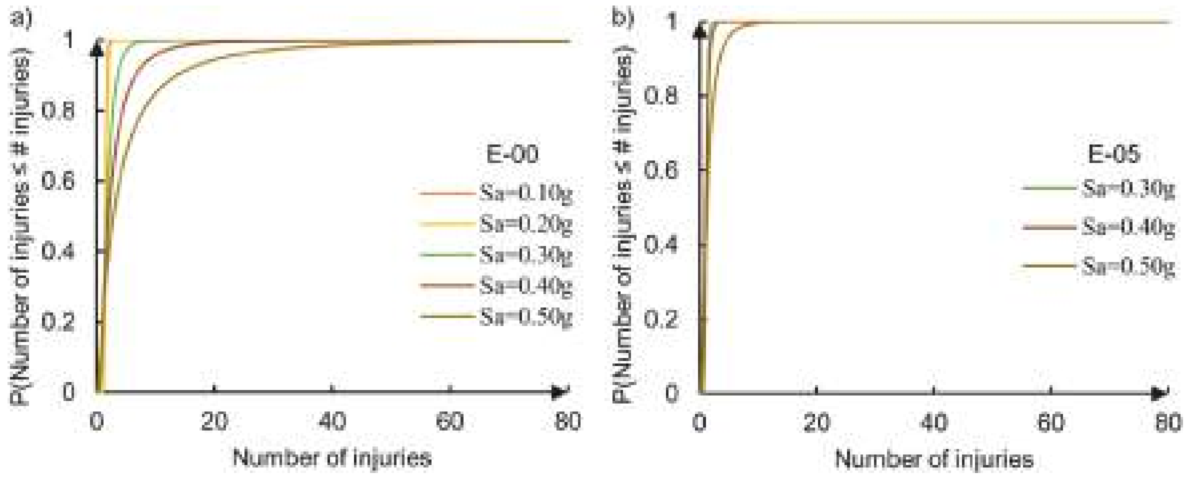

Fig. 12. Performance functions in terms of number of injured people for different levels of seismic intensity and for two case studies.

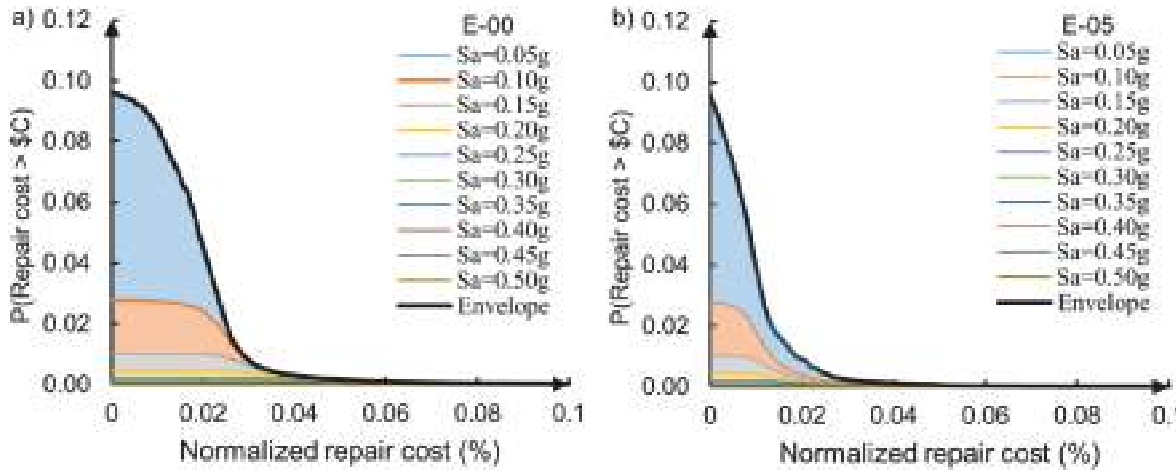

Fig. 13. Mean annual rate of exceedance in terms of normalized repair costs for two case studies: a) E−00, and b) E−05.

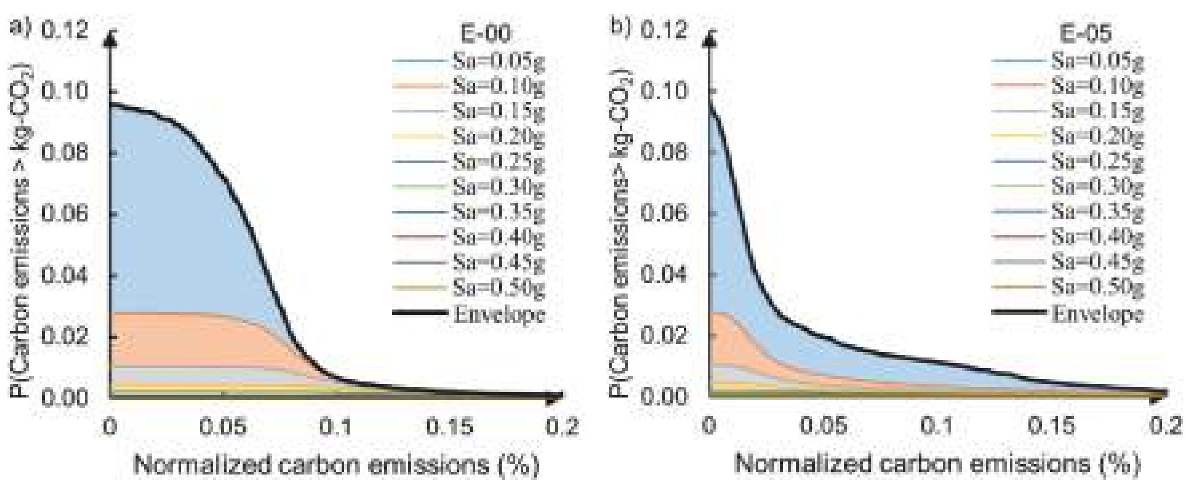

Fig. 14. Mean annual rate of exceedance in terms of normalized carbon emissions for two case studies: a) E−00, and b) E−05.

insurance premiums for future seismic events. The EAL is calculated as follows:

$$EAL = \int_0^\infty P(DV > dv)d(DV) \tag{7}$$

From a sustainability perspective, the optimal design is assumed to be the one that minimizes the expected annual loss in terms of repair costs, environmental impact (emissions of CO_2eq), and the number of injuries. As a result, Table 8 displays the expected annual losses for each of the case studies, calculated based on the performance variables

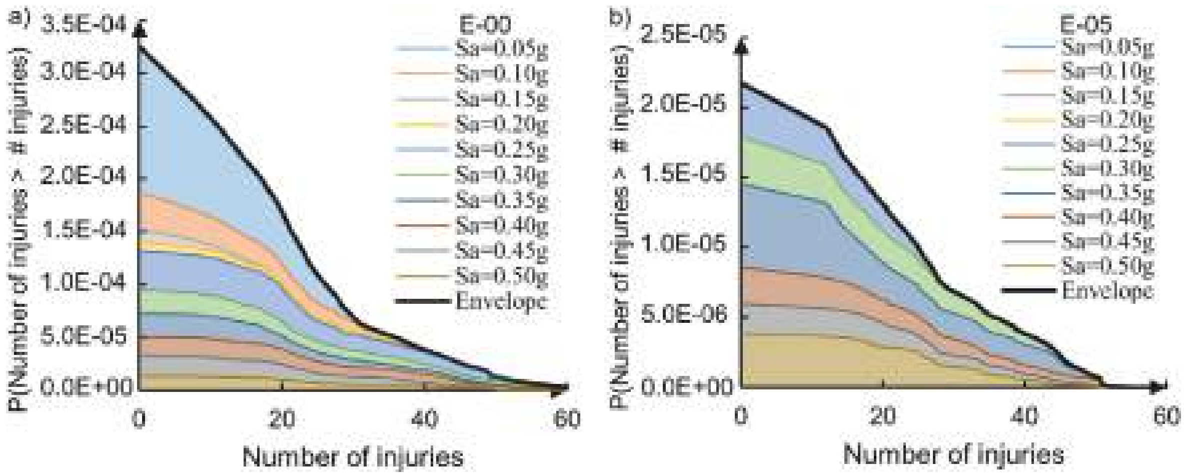

Fig. 15. Mean annual rate of exceedance in terms of the number of people injured for two case studies: a) E−00, and b) E−05.

Table 8
Expected annual loss due to repair costs, environmental impact, and the number of people injured.

Case studies	Repair cost ($)	Carbon emissions (kg-CO_2eq)	Serious injuries
E-00	0.208 %	0.66 %	0.00705
E-01	0.075 %	0.15 %	0.00030
E-02	0.075 %	0.13 %	0.00042
E-03	0.070 %	0.128 %	0.00024
E-04	0.15 %	0.22 %	0.00050
E-05	0.11 %	0.37 %	0.00054
E-06	0.20 %	0.59 %	0.00058
E-07	0.09 %	0.18 %	0.00104
E-08	0.09 %	0.14 %	0.00448
E-09	0.10 %	0.15 %	0.00636
E-10	0.10 %	0.18 %	0.00648

examined in this study.

It is worth noting that the expected annual losses for repair costs and carbon emissions were normalized based on the total cost of the building and the total amount of equivalent carbon dioxide emitted during the construction phase, respectively. As a result, case study E−03 ($\alpha = 0.3$) had the lowest losses across all performance variables considered and is thus established as the optimal design.

Regarding the E−03 model, the results show a significant reduction in annual losses of 65 % and 80 % for repair costs and environmental impact (Fig. 16a and b) compared to the building without an energy dissipation system (E−00). Additionally, the number of injuries also decreased substantially, although the expected annual loss for injuries was low for both cases.

On the other hand, concerning the structure without damping devices as a reference (E−00). The expected annual losses associated with repair costs are lower for those cases where the exponent α, which relates to the non-linearity of the damper, ranges from 0.1 to 0.3. Furthermore, estimated annual losses for structures with α values in this range (E−01 to E−03) are similar. This is evident in Fig. 16a, which displays the ratio between estimated annual losses for each case study with respect to the loss obtained for the reference structure. Conversely, when the exponent α takes values close to 0.4 and 0.6, the reductions compared to the reference case are less significant (see Fig. 16a).

The previously described trend in α values has been consistently reported in prior studies. For instance, Wang and Mahin [31] investigated the potential for retrofitting a 35-story existing steel building with fluid viscous dampers to minimize economic losses during a significant seismic event. Their research showed that nonlinear dampers with a damping exponent α of 0.35 effectively achieved structural control without generating excessive forces in either the dampers or structural elements. Additionally, Kolour et al. [108] introduced an algorithm for the optimal design of steel moment frames equipped with nonlinear viscous dampers with the aim of minimizing the total cost. Their findings indicated that the optimal damping exponent α fell within the range of 0.3–0.5 for the analyzed structures. Furthermore, Santos et al. [33]

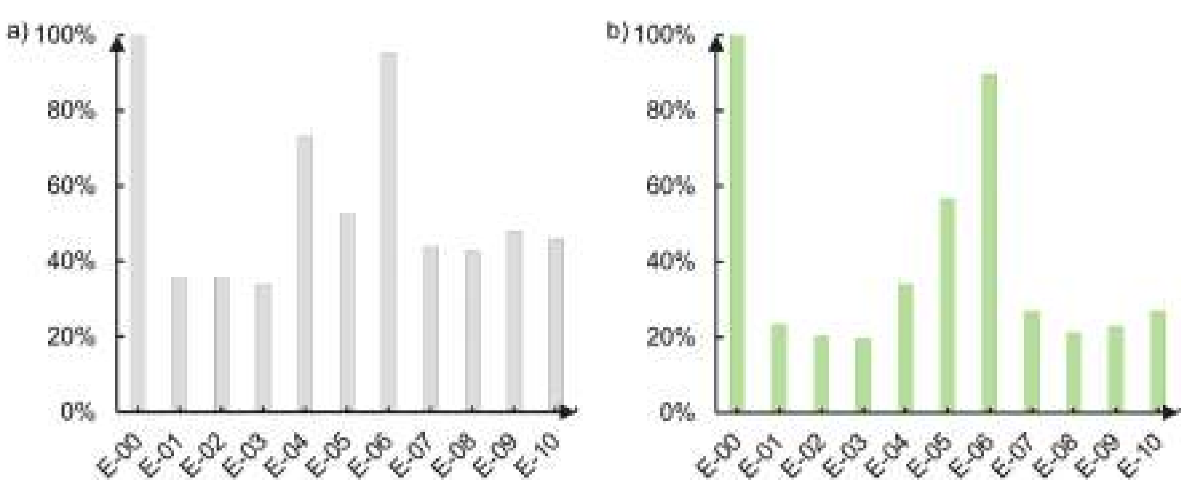

Fig. 16. Expected annual loss ratio between each case study and the reference case (E−00): a) repair costs, and b) carbon emissions.

presented a methodology for assessing the financial losses of steel-concrete composite frame structures equipped with fluid viscous dampers, considering seismic and wind hazards, cumulative structural damage, and repair-related downtime. Their findings revealed that the optimal design corresponds to structures with dampers, having a damping exponent α of 0.2 and a glass thickness of 10 mm.

Similarly, the expected annual losses attributable to environmental impact exhibit a similar pattern (refer to Fig. 16b). It is evident that the environmental impact is influenced by the repair costs, with higher repair costs usually leading to greater environmental impact, although this is not always the case. For instance, in the case of E−04 and E−05, where the estimated annual repair costs were 0.15 % and 0.11 %, respectively, the corresponding environmental impacts were 0.22 % and 0.37 %. This disparity can be attributed to the fact that the nonlinear response of buildings is different, therefore, the structural and non-structural components susceptible to being damaged are also different. Consequently, the repercussions for damaged components may be related to either a greater or a lower environmental impact.

Finally, the building structures equipped with damping systems (E−01 to E−10) exhibit lower expected annual losses associated with the number of injuries compared to the reference building (E−00). Nonetheless, it should be noted that these losses are deemed insignificant. This is because seismic design guidelines primarily prioritize life safety, and in this respect, these design guidelines achieve their intended purpose.

7. Conclusions

The aim of this research was to identify the optimal sustainable design for a set of building structures that included viscous fluid dampers. To create a range of design alternatives, the hysteretic properties of the devices were varied (α) and the seismic performance of each option was evaluated. The FEMA P-58 methodology was utilized to assess the seismic performance of the case studies in economic, social, and environmental terms. To achieve the three dimensions of sustainability, the seismic performance of each design was evaluated based on repair costs (economic), number of injuries (social), and carbon dioxide emissions (environmental impact). The optimal design was identified as the one with a specific value of α that minimized the expected annual loss based on the previously defined performance variables. According to the results, the following conclusions can be drawn:

- Time-based performance evaluation should primarily focus on moderate intensity values with less emphasis on high seismic intensity levels (relative to the seismic hazard of the place). This is due to the fact that the probability of exceeding a specific performance threshold is mostly influenced by moderate seismic intensity levels. A performance evaluation centered solely on high intensity levels could lead to underestimation of the results as significant information from the seismic hazard curve associated with low intensities would be omitted. Low intensities result in higher exceedance rates.
- The E−03 model ($\alpha = 0.3$) resulted in the case study with the lowest expected annual losses in terms of repair costs, environmental impact, and number of injuries, thus being determined as the optimal design. The results indicate a reduction in expected annual losses of 65 % and 80 % in terms of repair costs and carbon emissions, respectively, compared to the structure without an energy dissipation system (E−00). Additionally, there is a significant reduction in the number of injuries; however, the expected annual losses in both cases are minimal.
- In general, buildings with a viscous damping system (E−01 to E−10) have better seismic performance than those without an energy dissipation system (E−00). In this regard, the exponent $\boldsymbol{\alpha}$, related to the nonlinearity of the damper, has a significant influence on the performance of the analyzed cases. Structures with the highest performance indices are related to $\boldsymbol{\alpha}$ values between 0.1 and 0.3 (*i.e.*, E−01 to E−03). However, this conclusion corresponds to a high-rise building (28 levels) and to dynamic characteristics of a particular site (Acapulco, Gro.). Therefore, it is necessary to analyze structures of different heights and verify if indeed such $\boldsymbol{\alpha}$ values produce the best performance.
- Carbon emissions are strongly related to repair actions (*i.e.*, repair costs) and often, the higher the repair costs, the greater the environmental impact. However, the environmental impact produced in a structure with higher repair costs than another building may be lower due to the different response of the buildings. Therefore, the structural and non-structural components susceptible to damage are also different, and consequently, the repair actions of those components may generate more or less carbon emissions to the environment. On the other hand, Mexico has a scarce database to carry out life cycle analysis, therefore, life cycle inventories of developed countries were used to evaluate the environmental impact related to the construction sector. Regarding this issue, a national database is required to represent local materials and processes and thus characterize the environmental impact with greater certainty.
- Expected losses associated with the number of injuries are lower for buildings with a supplementary damping system (E−01 to E−10) compared to the building that does not include an energy dissipation system (E−00). Nevertheless, the expected losses related to the number of injuries are minimal for both systems. Certainly, current seismic design guidelines of structures prioritize life safety, thus, from this point of view, these design guidelines fulfill their objective.

Finally, it is important to point out the following:

- The widely used EIO-LCA method tends to overestimate the environmental impact, while Process-Based Life Cycle Analysis (PLCA) is more precise but less practical, requiring extensive data on product life cycle processes. A comprehensive comparison of EIO-LCA and PLCA, which includes adequate data to assess the environmental impact specifically for site of interest, would be valuable.
- The repair costs database in PACT was established for the United States. Despite adjustments made to account for the geographical location, some bias in the repair cost estimates may persist. A valuable approach would involve a comparative study that directly determines the economic consequences of damage states for the site of interest.
- Due to the scarcity of ground motion records in the area of study, a formal ground motion selection procedure was not feasible. A comparative study that considers multiple ground motion records from a similar region or even synthetic accelerograms would be worthy to assess the consistency of nonlinear displacement estimates.
- Since the highest performance indices are associated with α values between 0.1 and 0.3, a comparative study of viscous dampers with different damping constants and damper locations, all characterized by exponents in the range of 0.1 and 0.3, would be of great interest.

CRediT authorship contribution statement

Ali Rodríguez-Castellanos: Formal analysis, Investigation, Methodology, Software, Writing – original draft. **Mauro Niño:** Data curation, Funding acquisition, Project administration, Resources, Supervision, Validation, Visualization, Writing – review & editing. **Sonia E. Ruiz:** Data curation, Investigation, Methodology, Supervision, Writing – review & editing. **Marco A. Santos Santiago:** Methodology, Resources, Software.

Declaration of competing interest

By this mean, I declare that I and the coauthors have no significant competing financial, professional, or personal interests that might have influenced the performance or presentation of the work described in the manuscript entitle **"*Multi-disciplinary performance comparison for selecting the optimal sustainable design of buildings structures with fluid-viscous dampers*"**, prepared to be submitted to the Soil Dynamics and Earthquake Engineering journal by Ali Rodríguez-Castellanos, Mauro Niño, Sonia E. Ruiz and Marco A. Santos Santiago.

Data availability

No data was used for the research described in the article.

Acknowledgements

The first author expresses gratitude to the Universidad Nacional Autónoma de México (UNAM) for the support provided through its "Programa de Becas Posdoctorales en la UNAM", which is coordinated by the Dirección General de Asuntos del Personal Académico (DGAPA). The second author would like to acknowledge the support received from the Consejo Nacional de Ciencia y Tecnología (CONACYT) for sponsoring the project A1-S-35223: "Definition of seismic demands for the design of structures based on hazard and resilience". Finally, the authors would like to express their gratitude to the three anonymous reviewers who contributed to improve the quality of the paper.

References

[1] American Society of Civil Engineers (ASCE). Minimum design loads and associated criteria for buildings and other structures (ASCE/SEI 7-16). Reston, VA: American Society of Civil Engineers; 2017. https://doi.org/10.1061/9780784414248.
[2] Gobierno de la Ciudad de Mexico (GCDMX). Normas técnicas complementarias para diseño por sismo. Ciudad de México: Gobierno de la Ciudad de Mexico; 2020.
[3] Applied Technology Council (ATC). Seismic evaluation and retrofit of concrete building (ATC-40). Redwood City, CA: Applied Technology Council; 1996.
[4] Federal Emergency Management Agency (FEMA). NEHRP guidelines for the seismic rehabilitation of buildings. Washington, D.C.: Rep. No. FEMA-273; 1997.
[5] Ghobarah A. Performance-based design in earthquake engineering: state of development. Eng Struct 2001;23:878–84. https://doi.org/10.1016/S0141-0296(01)00036-0.
[6] American Society of Civil Engineers (ASCE). Seismic evaluation and retrofit of existing buildings. Reston, VA: American Society of Civil Engineers; 2017. ASCE/SEI 41-17), https://doi/book/10.1061/9780784414859.
[7] Comber MV, Poland C, Sinclair M. Environmental Impact Seismic Assessment: Application of Performance-Based Earthquake Engineering Methodologies to Optimize Environmental Performance. In: Proceedings of the Structures Congress ASCE, Chicago, IL, USA, pp. 910-921. https://doi.org/10.1061/9780784412367.081..
[8] Feese C, Li Y, Bulleit WM. Assessment of seismic damage of buildings and related environmental impacts. J Perform Constr Facil 2015;29:1–10. https://doi.org/10.1061/(asce)cf.1943-5509.0000584.
[9] Hossain KA, Gencturk B. Life-cycle environmental impact assessment of reinforced concrete buildings subjected to natural hazards. J Architect Eng 2016;22. https://doi.org/10.1061/(ASCE)AE.1943-5568.0000153.
[10] Salgado RA, Apul D, Guner S. Life cycle assessment of seismic retrofit alternatives for reinforced concrete frame buildings. J Build Eng 2020;28:101064. https://doi.org/10.1016/j.jobe.2019.101064.
[11] Architecture 2030. Why the building sector?. http://architecture2030.org/buildings_problem_why/; 2023.
[12] Menna C, Asprone D, Jalayer F, Prota A, Manfredi G. Assessment of ecological sustainability of a building subjected to potential seismic events during its lifetime. Int J Life Cycle Assess 2013;18:504–15. https://doi.org/10.1007/s11367-012-0477-9.
[13] Wei H-H, Skibniewski MJ, Shohet IM, Yao X. Lifecycle environmental performance of natural-hazard mitigation for buildings. J Perform Constr Facil 2016;30:1–13. https://doi.org/10.1061/(asce)cf.1943-5509.0000803.
[14] Salgado RA, Guner S. A structural performance-based environmental impact assessment framework for natural hazard loads. J Build Eng 2021;43:102908. https://doi.org/10.1016/j.jobe.2021.102908.
[15] Federal Emergency Management Agency (FEMA). Seismic performance assessment of buildings, volume1-methodology. Washington, DC: Rep. No. FEMA P-58-1; 2018.
[16] Dong Y, Frangopol DM. Performance-based seismic assessment of conventional and base-isolated steel buildings including environmental impact and resilience. Earthq Eng Struct Dynam 2016;45:739–56. https://doi.org/10.1002/eqe.2682.
[17] Gencturk B, Hossain K, Lahourpour S. Life cycle sustainability assessment of RC buildings in seismic regions. Eng Struct 2016;110:347–62. https://doi.org/10.1016/j.engstruct.2015.11.037.
[18] Park HS, Hwang JW, Oh BK. Integrated analysis model for assessing CO2 emissions, seismic performance, and costs of buildings through performance-based optimal seismic design with sustainability. Energy Build 2018;158:761–75. https://doi.org/10.1016/j.enbuild.2017.10.070.
[19] Passoni C, Marini A, Belleri A, Menna C. Redefining the concept of sustainable renovation of buildings: state of the art and an LCT-based design framework. Sustain Cities Soc 2021;64:102519. https://doi.org/10.1016/j.scs.2020.102519.
[20] Cardone D, Gesualdi G, Perrone G. Cost-benefit analysis of alternative retrofit strategies for RC frame buildings. J Earthq Eng 2019;23:208–41. https://doi.org/10.1080/13632469.2017.1323041.
[21] Del Gobbo GM, Williams MS, Blakeborough A. Seismic performance assessment of Eurocode 8-compliant concentric braced frame buildings using FEMA P-58. Eng Struct 2018;155:192–208. https://doi.org/10.1016/j.engstruct.2017.11.016.
[22] Güner T, Topkaya C. Performance comparison of BRBFs designed using different response modification factors. Eng Struct 2020;225. https://doi.org/10.1016/j.engstruct.2020.111281.
[23] Khalilian M, Shakib H, Basim MC. On the optimal performance-based seismic design objective for steel moment resisting frames based on life cycle cost. J Build Eng 2021;44. https://doi.org/10.1016/j.jobe.2021.103091.
[24] Yekrangnia M, Bakhshi A, Ghannad MA, Panahi M. Risk assessment of confined unreinforced masonry buildings based on FEMA P-58 methodology: a case study—school buildings in Tehran, vol. 19. Springer Netherlands; 2021. https://doi.org/10.1007/s10518-020-00990-1.
[25] Ghasemof A, Mirtaheri M, Karami Mohammadi R. Multi-objective optimization for probabilistic performance-based design of buildings using FEMA P-58 methodology. Eng Struct 2022;254. https://doi.org/10.1016/j.engstruct.2022.113856.
[26] Constantinou MC, Tsopelas P, Hammel W, Sigaher AN. Toggle-brace-damper seismic energy dissipation systems. J Struct Eng 2001;127:105–12. https://doi.org/10.1061/(ASCE)0733-9445(2001)127:2(105).
[27] Soong TT, Spencer BF. Supplemental energy dissipation: state-of-the-art and state-of-the-practice. Eng Struct 2002;24:243–59. https://doi.org/10.1016/S0141-0296(01)00092-X.
[28] Banazadeh M, Ghanbari A, Ghanbari R. Seismic performance assessment of steel moment-resisting frames equipped with linear and nonlinear fluid viscous dampers with the same damping ratio. J Constr Steel Res 2017;136:215–28. https://doi.org/10.1016/j.jcsr.2017.05.022.
[29] Del Gobbo GM, Blakeborough A, Williams MS. Improving total-building seismic performance using linear fluid viscous dampers. Bull Earthq Eng 2018;16:4249–72. https://doi.org/10.1007/s10518-018-0338-4.
[30] Dimopoulos AI, Tzimas AS, Karavasilis TL, Vamvatsikos D. Probabilistic economic seismic loss estimation in steel buildings using post-tensioned moment-resisting frames and viscous dampers. Earthq Eng Struct Dynam 2016;45:1725–41. https://doi.org/10.1002/eqe.2722.
[31] Wang S, Mahin SA. Seismic retrofit of a high-rise steel moment-resisting frame using fluid viscous dampers. Struct Des Tall Special Build 2017;26. https://doi.org/10.1002/tal.1367.
[32] Del Gobbo GM, Williams MS, Blakeborough A. Comparing fluid viscous damper placement methods considering total-building seismic performance. Earthq Eng Struct Dynam 2018;47:2864–86. https://doi.org/10.1002/eqe.3117.
[33] Santos-Santiago MA, Ruiz SE, Cruz-Reyes L. Optimal design of buildings under wind and earthquake, considering cumulative damage. J Build Eng 2022;56:104760. https://doi.org/10.1016/j.jobe.2022.104760.
[34] De Silva CW. An algorithm for the optimal design of passive vibration controllers for flexible systems. J Sound Vib 1981;75:495–502. https://doi.org/10.1016/0022-460X(81)90437-5.
[35] Zhang R, Soong TT. Seismic design of viscoelastic dampers for structural applications. J Struct Eng 1992;118:1375–92. https://doi.org/10.1061/(ASCE)0733-9445(1992)118:5(1375).
[36] Takewaki I. Optimal damper placement for minimum transfer functions. Earthq Eng Struct Dynam 1997;26:1113–24. https://doi.org/10.1002/(SICI)1096-9845(199711)26:11<1113::AID-EQE696>3.0.CO;2-X.
[37] Shen KL, Soong TT. Design of energy dissipation devices based on concept of damage control. J Struct Eng 1996;122:76–82. https://doi.org/10.1061/(asce)0733-9445(1996)122:1(76).
[38] Gluck N, Reinhorn AM, Gluck J, Levy R. Design of supplemental dampers for control of structures. J Struct Eng 1996;122:1394–9. https://doi.org/10.1061/(asce)0733-9445(1996)122:12(1394).
[39] Constantinou MC, Symans MD. Experimental and analytical investigation of seismic response of structures with supplemental fluid viscous dampers. In: Technical report NCEER-92-0032, national center for earthquake enginering research (NCEER). NY: State University of New York at Buffalo; 1992.
[40] Cimellaro GP. Design optimization of active and passive structural control systems. IGI Global; 2013. https://doi.org/10.4018/978-1-4666-2029-2.
[41] Takewaki I. Building control with passive dampers: optimal performance-based design for earthquakes. Singapore: Jhon Wiley & Sons; 2009. https://doi.org/10.1002/9780470824931.
[42] Christopoulos C, Filiatrault A. Principles of passive supplemental damping and seismic isolation. Pavia, Italy: IUSS Press; 2006.
[43] De Domenico D, Ricciardi G, Takewaki I. Design strategies of viscous dampers for seismic protection of building structures: a review. Soil Dynam Earthq Eng 2019;118:144–65. https://doi.org/10.1016/j.soildyn.2018.12.024.
[44] García DL. A simple method for the design of optimal damper configurations in MDOF structures. Earthq Spectra 2001;17:387–98. https://doi.org/10.1193/1.1586180.

[45] Kim J, Choi H, Min KW. Performance-based design of added viscous dampers using capacity spectrum method. J Earthq Eng 2003;7:1–24. https://doi.org/10.1080/13632460309350439.

[46] Uetani K, Tsuji M, Takewaki I. Application of an optimum design method to practical building frames with viscous dampers and hysteretic dampers. Eng Struct 2003;25:579–92. https://doi.org/10.1016/S0141-0296(02)00168-2.

[47] Silvestri S, Gasparini G, Trombetti T. A five-step procedure for the dimensioning of viscous dampers to be inserted in building structures. J Earthq Eng 2010;14:417–47. https://doi.org/10.1080/13632460903093891.

[48] Zhou Y, Lu X, Weng D, Zhang R. A practical design method for reinforced concrete structures with viscous dampers. Eng Struct 2012;39:187–98. https://doi.org/10.1016/j.engstruct.2012.02.014.

[49] Landi L, Fabbri O, Diotallevi PP. A two-step direct method for estimating the seismic response of nonlinear structures equipped with nonlinear viscous dampers. Earthq Eng Struct Dynam 2014;43:1641–59. https://doi.org/10.1002/eqe.2415.

[50] Palermo M, Silvestri S, Landi L, Gasparini G, Trombetti T. A "direct five-step procedure" for the preliminary seismic design of buildings with added viscous dampers. Eng Struct 2018;173:933–50. https://doi.org/10.1016/j.engstruct.2018.06.103.

[51] Gherbi A, Belgasmia M. A simplified design strategy of nonlinear fluid viscous dampers for MDOF structures. Iran J Sci Technol - Trans Civ Eng 2022;46:857–64. https://doi.org/10.1007/s40996-021-00635-6.

[52] European Committee for Standardization (CEN). European standard EN 15129 for anti-seismic devices. 2009.

[53] Japan Society of Seismic Isolation (JSSI). Manual, design and construction manual for passively controlled buildings. second ed. Tokyo, Japan: Second Print; 2007.

[54] Building Seismic Safety Council (BSSC). NEHRP recommended provisions for seismic regulations for new buildings and other structures (FEMA 450). Edition, Part 1. Washington, DC: Provisions; 2003. 2004.

[55] Comision Federal de Electricidad (CFE). Manual de Diseño de Obras Civiles Diseño por Sismo. Mexico: Instituto de Investigaciones Eléctricas, Comisión Federal de Electricidad, Ciudad de Mexico; 2015.

[56] Santos-Santiago MA, Ruiz SE, Valenzuela-Beltrán F. Influence of higher modes of vibration on the seismic response of buildings with linear and nonlinear viscous dampers. J Earthq Eng 2022;26:3914–37. https://doi.org/10.1080/13632469.2020.1822223.

[57] Lin WH, Chopra AK. Earthquake response of elastic SDF systems with non-linear fluid viscous dampers. Earthq Eng Struct Dynam 2002;31:1623–42. https://doi.org/10.1002/eqe.179.

[58] Santos-Santiago MA, Ruiz SE, Santos-Santiago A, Valenzuela Beltrán F. Comparación de dos metodos simplificados para el diseño sísmico de edificios con amortiguadores viscosos no lineales. In: Proceedings of the XXI congreso nacional de Ingeneria sísmica. Mexico: Guadalajara, Jalisco; 2017 (in Spanish).

[59] Santos-Santiago A, Ruiz SE, Santos-Santiago MA. Comparación de dos métodos para calcular la constante de amortiguamiento de disipadores viscosos. In: Proceedings of the XXII congreso nacional de Ingeneria sísmica. Mexico: Monterrey, Nuevo León; 2019 (in Spanish).

[60] Ruiz SE, Santos-Santiago MA, Valenzuela-Beltrán F. Comparison of guidelines for seismic design of structures with passive energy dissipation devices. In: Proceedings of the 6th struct eng world congr. Cancun. Mexico: Quintana Roo; 2017.

[61] Ramirez OM, Constantinou MC, Kircher CA, Whittaker A, Johnson M, Gomez JD, et al. Development and Evaluation of simplified procedures for analysis and design of buildings with passive energy dissipation systems. Technical Rep. No. MCEER-00–0010, Revision, 1; 2001.

[62] Cornell CA, Krawinkler H. Progress and challenges in seismic performance assessment. PEER Cent News 2000;3:1–4.

[63] Moehle J, Deierlein GG. A framework methodology for performance-based earthquake engineering. In: Proceedings of the 13th world conference on earthquake engineering; 2004. Vancouver, BC, Canada.

[64] Yang TY, Moehle J, Stojadinovic B, Der Kiureghian A. Seismic performance evaluation of facilities: methodology and implementation. J Struct Eng 2009;135:1146–54. https://doi.org/10.1061/(asce)0733-9445(2009)135:10(1146).

[65] Vamvatsikos D, Allin Cornell C. Incremental dynamic analysis. Earthq Eng Struct Dynam 2002;31:491–514. https://doi.org/10.1002/eqe.141.

[66] Federal Emergency Management Agency (FEMA). Seismic performance assessment of buildings, volume 3- supporting materials and background documentation. Washington, DC, USA: Rep. No. FEMA P-58-3; 2018.

[67] Huang M, Simonen K. Methodology for environmental impact assessment. Background document: FEMA P-58/BD-3.7.20. 2018. Washington, DC, USA.

[68] Hasik V, Chhabra JPS, Warn GP, Bilec MM. Review of approaches for integrating loss estimation and life cycle assessment to assess impacts of seismic building damage and repair. Eng Struct 2018;175:123–37. https://doi.org/10.1016/j.engstruct.2018.08.011.

[69] Carnegie Mellon University Green Design Institute (CMU GDI). Economic input-output life cycle assessment (EIO-LCA), US 1997 industry benchmark model. Retrieved. 2008. from, http://www.eiolca.net. [Accessed 22 November 2022].

[70] Yang Y, Ingwersen WW, Hawkins TR, Srocka M, Meyer DE. USEEIO: a new and transparent United States environmentally-extended input-output model. J Clean Prod 2017;158:308–18. https://doi.org/10.1016/j.jclepro.2017.04.150.

[71] Güereca LP, Sosa RO, Gilbert HE, Reynaga NS. Life cycle assessment in Mexico: overview of development and implementation. Int J Life Cycle Assess 2015;20:311–7. https://doi.org/10.1007/s11367-014-0844-9.

[72] Quispe I, Vázquez-Rowe I, Kahhat R, Arena AP, Suppen N. Preface. Int J Life Cycle Assess 2017;22:469–78. https://doi.org/10.1007/s11367-016-1178-6.

[73] Reynaga N, Aguillón Robles J, Arista González GJ. Análisis de Ciclo de Vida y Ecodiseño para la Construcción en México. PhD Thesis. UASLP, México; 2013 (in Spanish).

[74] Contreras-Jiménez JC, Morales-Mendoza F, Corona-Armenta R, Montaño-Arango O, Medina-Marín J. Evaluación económica y ambiental de diseños estructurales de edificaciones mediante análisis de ciclo de vida basado en entradas y salidas. Dyna 2017;92:626–31. https://doi.org/10.6036/8177.

[75] Colín IF. Aplicacion de analisis de ciclo vida para un edificio residencial con criterios de sustentabilidad. PhD Thesis. Mexico: IPN; 2020 (in Spanish), http://tesis.ipn.mx/handle/123456789/28847.

[76] Simonen K, Huang M, Aicher C, Morris P. Embodied carbon as a proxy for the environmental impact of earthquake damage repair. Energy Build 2018;164:131–9. https://doi.org/10.1016/j.enbuild.2017.12.065.

[77] Servicio Sismologico Nacional (SSN). Mapas de sismicidad anual. http://www.ssn.unam.mx/sismicidad/mapas-de-sismicidad-anual/; 2023.

[78] Lu Z, He X, Zhou Y. Performance-based seismic analysis on a super high-rise building with improved viscously damped outrigger system. Struct Control Health Monit 2018;25:1–21. https://doi.org/10.1002/stc.2190.

[79] Simonen K, Merrifield S, Almufti I, Strobel K, Tipler J. Integrating environmental impacts as another measure of earthquake performance for tall buildings in high seismic zones. In: Struct. Congr. Reston, VA: American Society of Civil Engineers; 2015. p. 933–44. https://doi.org/10.1061/9780784479117.080. 2015.

[80] Computers and Structures Inc. (CSI). Structural software for building analysis and design. ETABS; 2018.

[81] United States Government (USG). CPI inflation calculator, U.S. Bureau of labor Statistics. https://www.bls.gov/data/inflation_calculator.htm; 2023.

[82] Seligson HA. Background document casualty consequence function and building population model development. Background document: FEMA P-58/BD-3.7.8. 2008. Washington, DC, USA.

[83] Baker JW. Efficient analytical fragility function fitting using dynamic structural analysis. Earthq Spectra 2015;31:579–99. https://doi.org/10.1193/021113EQS025M.

[84] Lowes LN, Li J. Fragility functions for reinforced concrete moment frames. 2009. Background document: FEMA P-58/BD-3.8.6, Washington, DC, USA.

[85] Deierlein G, Victorsson V. Fragility curves for components of steel SMF systems. 2009. Background document: FEMA P-58/BD-3.8.3. Washington, DC, USA.

[86] Federal Emergency Management Agency (FEMA). Interim testing protocols for determining the seismic performance characteristics of structural and nonstructural components. Washington, DC, USA: Rep. No. FEMA 461; 2007.

[87] Miyamoto HK, Gilani ASJ, Wada A, Ariyaratana C. Collapse risk of tall steel moment frame buildings with viscous dampers subjected to large earthquakes-Part I: damper limit states and failure modes of 10-storey archetypes. Struct Des Tall Special Build 2010;19:421–38. https://doi.org/10.1002/tal.593.

[88] Porter K, Farokhnia K, Vamvatsikos D, Cho I. Guidelines for component- based analytical vulnerability assessment of buildings and nonstructural elements. GEM technical report 2014-13, version 1.0.0. Pavia: Global Earthquake Model; 2015.

[89] Silva A, Castro JM, Monteiro R. A rational approach to the conversion of FEMA P-58 seismic repair costs to Europe. Earthq Spectra 2020;36:1607–18. https://doi.org/10.1177/8755293019899964.

[90] Turner, Townsend. International construction market survey, Turner and Townsend. 2021. p. 69.

[91] Carrillo-Bueno CA. Influencia del deterioro por corrosión en la confiabilidad de edificios de concreto reforzado. PhD Thesis. Mexico: UNAM; 2016 (in Spanish).

[92] Rodríguez-Castellanos A, Ruiz SE, Bojórquez E, Reyes-Salazar A. Influence of spectral acceleration correlation models on conditional mean spectra and probabilistic seismic hazard analysis. Earthq Eng Struct Dynam 2020. https://doi.org/10.1002/eqe.3331. eqe.3331.

[93] Baker JW. Conditional mean spectrum: tool for ground-motion selection. J Struct Eng 2011;137:322–31. https://doi.org/10.1061/(ASCE)ST.1943-541X.0000215.

[94] Singh SK, Cruz-Atienza V, Pérez-Campos X, Iglesias A, Hjörleifsdóttir V, Reinoso E, et al. Deadly intraslab Mexico earthquake of 19 September 2017 (Mw 7.1): ground motion and damage pattern in Mexico City. Seismol Res Lett 2018;89:2193–203. https://doi.org/10.1785/0220180159.

[95] García D, Singh SK, Herráiz M, Pacheco JF, Ordaz M. Inslab earthquakes of Central Mexico: Q, source spectra, and stress drop. Bull Seismol Soc Am 2004;94:789–802. https://doi.org/10.1785/0120030125.

[96] Singh SK, Ordaz M, Pérez-Campos X, Iglesias A. Intraslab versus interplate earthquakes as recorded in Mexico City: Implications for seismic hazard. Earthq Spectra 2015;31:795–812. https://doi.org/10.1193/110612EQS324M.

[97] Günay S, Mosalam KM. PEER performance-based earthquake engineering methodology, revisited. J Earthq Eng 2013;17:829–58. https://doi.org/10.1080/13632469.2013.787377.

[98] Baker JW, Cornell CA. Spectral shape, epsilon and record selection. Earthq Eng Struct Dynam 2006;35:1077–95. https://doi.org/10.1002/eqe.571.

[99] Bianchini M, Diotallevi PP, Baker JW. Prediction of inelastic structural response using an average of spectral accelerations. In: Proceedings of the 10th international conference on structural safety and reliability (ICOSSAR09). Osaka: Japon; 2009.

[100] Tsantaki S, Jäger C, Adam C. Improved seismic collapse prediction of inelastic simple systems vulnerable to the P-delta effect based on average spectral acceleration. In: Proceedings of the 15th world conference on earthquake engineering. Lisbon: Portugal; 2012.

[101] Eads L, Miranda E, Lignos DG. Average spectral acceleration as an intensity measure for collapse risk assessment. Earthq Eng Struct Dynam 2015;44:2057–73. https://doi.org/10.1002/eqe.2575.

[102] Kazantzi AK, Vamvatsikos D. Intensity measure selection for vulnerability studies of building classes. Earthq Eng Struct Dynam 2015;44:2677–94. https://doi.org/10.1002/eqe.2603.

[103] Kohrangi M, Kotha SR, Bazzurro P. Ground-motion models for average spectral acceleration in a period range: direct and indirect methods. Bull Earthq Eng 2018;16:45–65. https://doi.org/10.1007/s10518-017-0216-5.

[104] Carr A J. Ruaumoko Manual: User Manual for the 3 Dimensional Version Ruaumoko 3D. Unversity of Cantebury, Christchurch, NZ. https://doi.org/10.13140/RG.2.1.4755.8567..

[105] Ramberg W, Osgood WR. Description of stress-strain curves by three parameters. Technical note No. 902. Washington, DC, USA: National Advisory Committee on Aeronautics; 1943.

[106] Takeda T, Sozen MA, Nielsen NN. Reinforced concrete response to simulated earthquakes. J Struct Div 1970;96:2557–73. https://doi.org/10.1061/JSDEAG.0002765.

[107] Alehojjat SB, Yakhchalian M, Bahar O. Approximate methods to estimate residual drift demands in steel structures with viscous dampers designed by the DDBD approach. Int J Steel Struct 2023;23:806–22. https://doi.org/10.1007/s13296-023-00732-4.

[108] Ahadzadeh Kolour N, Charkhtab Basim M, Chenaghlou M. Multi-objective optimum design of nonlinear viscous dampers in steel structures based on life cycle cost. Structures 2021;34:3776–88. https://doi.org/10.1016/j.istruc.2021.09.100.